Resource sharing by outer membrane vesicles from a citrus pathogen

Gabriel G. Araujo[1], Matheus M. Conforte[1], Aline D. da Purificação[1], Iris Todeschini[1], Edgar E. Llontop[2], Claudia B. Angeli[3], Alex Inague[2], Marcos Y. Yoshinaga[2], Robson F. de Souza[1], Rodrigo Papai[4], Maciel S. Luz[4], Sayuri Miyamoto[2], Giuseppe Palmisano[3], Chuck S. Farah[2], Cristiane R. Guzzo[1#]

[1] Department of Microbiology, Institute of Biomedical Sciences, University of São Paulo, Ave. Prof. Lineu Prestes, 1374, Cidade Universitária, 05508-000, São Paulo, SP, Brazil.

[2] Department of Biochemistry, Institute of Chemistry, University of São Paulo, Ave. Prof. Lineu Prestes, 748, Cidade Universitária, 05508-000, São Paulo, SP, Brazil.

[3] Department of Parasitology, Institute of Biomedical Sciences, University of São Paulo, Ave. Prof. Lineu Prestes, 1374, Cidade Universitária, 05508-900, São Paulo, SP, Brazil.

[4] Laboratório de Processos Metalúrgicos, Instituto de Pesquisas Tecnológicas do Estado de São Paulo (IPT), Ave. Prof. Almeida Prado, 532, Cidade Universitária, 05508-901, São Paulo, SP, Brazil.

To whom correspondence should be addressed: Prof. Cristiane Guzzo Carvalho, Department of Microbiology, Institute of Biomedical Sciences, University of São Paulo, Ave. Prof. Lineu Prestes, 1374, Cidade Universitária, 05508-000, São Paulo, SP, Brazil, phone: +55 11 3091-7298; email: crisguzzo@usp.br and crisguzzo@gmail.com.

Running title: Resource sharing by OMVs

Abstract

The causative agent of citrus canker disease, *Xanthomonas citri* pv. *citri*, was found to produce copious amounts of outer membrane vesicles (OMVs), frequently forming long membranous tubes under different culture conditions. Lipidomic analysis revealed significant differences in lipid composition between purified vesicles in relation to whole cells. The results suggest an enrichment in saturated cardiolipins and a decrease in unsaturated lipids in the OMV samples, possibly granting them a more rigid structure while allowing their high degree of curvature caused by their small diameters. The vesicles' proteome was found to be significantly enriched in TonB-dependent receptors related to the acquisition of different nutrients. These proteins are known to transport siderophores, which were evidenced to be present in purified *X. citri* OMVs, along with essential metals including iron, zinc, and manganese quantified by elemental analysis. The availability of vesicle-associated nutrients to be incorporated by cells was demonstrated by the use of OMVs as the sole carbon source for bacterial growth. At last, the vesicles also presented esterase and protease activities, which have been associated with virulence in phytopathogens. These evidences point that *X. citri* cells can use OMVs to share resources within microbial communities, which has potential implications for microbial interactions and plant colonization, affecting their survival and persistence on the host and in the environment.

Importance

The shedding of outer membrane vesicles appears to be universal in Gram-negative bacteria and effectively constitutes a unique secretion pathway for diverse molecules and proteins. To study their possible functions in the citrus pathogen *Xanthomonas citri*, purified

47 vesicles from this bacterium were studied by omics and functional approaches. Nutrient
48 transporters were found associated to these structures, which were evidenced to contain
49 siderophores and essential metals. The availability of these nutrients to be incorporated by cells
50 was then demonstrated by showing that purified vesicles can be used as sole carbon sources for
51 microbial growth. Additionally, the samples also presented esterase and protease activities which
52 can contribute to the release of substrates from plant host tissues. These observations help to
53 establish the developing idea of vesicles as shared bacterial resources which can participate in
54 shaping host-associated microbial communities in contrast to other interactions such as bacterial
55 competition.
56
57 **Introduction**
58 The production of outer membrane vesicles (OMVs) is known to be extremely common
59 to Gram-negative bacteria and has been specially explored in pathogens due to their association
60 to virulence factors (Schwechheimer and Kuehn, 2015; Toyofuku et al., 2019). Less commonly
61 described structures are outer membrane tubes, also named tube-shaped membranous structures,
62 nanotubes, nanowires and nanopods in different organisms. The tubes are considered to be a
63 specialized form of OMVs, which assemble in the form of chains or completely fused to one
64 another (Pirbadian et al., 2014; Remis et al., 2014; Pirbadian et al., 2015; Fischer et al., 2019;
65 Toyofuku et al., 2019). These tubes seem to have the potential to bridge cell surfaces at long
66 ranges, but their exact function, if at all dependent on their elongated shape, is still unclear on
67 most cases and varies between different organisms.
68 *Myxococcus xanthus* outer membrane tubes are some of the most studied of these
69 structures, forming a widespread network between the cells within biofilms that were proposed

to promote coordination for these bacteria's notorious social behaviors by serving as a transport medium for proteins and other molecules (Remis et al., 2014). Nevertheless, simply the presence of the tubes may not be sufficient for such activities since specific factors were found to be necessary to allow effective molecular exchanges through outer membrane connections. Namely, the proteins TraA and TraB were identified by genetic screening to be required for transferring outer membrane proteins by direct contacts between cells, while not affecting the production of tubes (Dey and Wall, 2014; Cao and Wall, 2019). In the zoonotic pathogen *Francisella novicida* which causes tularemia disease, virulence factors were detected in its OMVs and outer membrane tubes, which interestingly always appear to be of a continuous, non-segmented type. Interaction with host cells led to increased expression of the tubes, suggesting a role of these structures in the infection process (McCaig et al., 2013; Sampath et al., 2018). In *Vibrio vulnificus,* OMVs carry the virulence factor cytolysin–hemolysin VvhA (Kim et al., 2010), while its segmented tubes seem to exist only transiently as intermediates within the capsule of this opportunistic pathogen (Hampton et al., 2017). Somewhat in contrast to these examples, the outer membrane tubes of *Shewanella oneidensis* seem play a much clearer role in the biology of this organism. These membranous extensions form "nanowires" from which components of the electron transport chain of this metal-reducing bacterium can reach extracellular mineral electron acceptors (Pirbadian et al., 2014, 2015).

Studies with other environmental bacteria also revealed other possible implications of these structures on cell metabolism. In a marine *Flavobacterium* sp., OMV chains were proposed to serve as an extension of the cell surface for the degradation and incorporation of substrates (Fischer et al., 2019). OMVs of polycyclic aromatic hydrocarbon-degrading *Delftia* sp. Cs1-4 were found to be contained within tubular "nanopods" surrounded by a surface layer protein,

NpdA, the production of which was stimulated by growth on phenanthrene. The presence of NpdA and the formation of an encasing structure for OMV tubes seem to be a characteristic distributed within the *Comamonadaceae* family (Shetty et al., 2011).

The examples presented above represent some of the exploration done on the relatively few, but nonetheless diverse bacteria identified that assemble extracellular tubular-shaped structures from their outer membrane. Nevertheless, OMVs are most commonly found not as chains but as free entities, which are produced by Gram-negative bacteria in different environments, such as biofilms, planktonic cultures, and within hosts (Hellman et al., 2000; Biller et al., 2014; Hickey et al., 2015). More generally speaking, extracellular membrane vesicles are also commonly produced by Gram-positive bacteria, archaea, and by eukaryotic cells (Schwechheimer and Kuehn, 2015).

Due to them being an effective way for microbial cells to release the most diverse compounds, OMV production can be used as a secretion mechanism and thus have been called the “type zero secretion system” (Schwechheimer and Kuehn, 2015; Guerrero-Mandujano et al., 2017; Toyofuku et al., 2019). Differently from other bacterial secretion systems, OMVs require a remodeling of the Gram-negative envelope to release vesicles made of outer membrane constituents with a periplasmic lumen. Therefore, different bacterial envelope crosslinks and non-covalent interactions between proteins located in the membrane that interact with the cell wall must be broken during the secretion of OMVs (Schwechheimer and Kuehn, 2015). Details of this process are still unclear, as well as if there is any generalized protein system actively involved in OMV biogenesis. Another process that is still not well understood is cargo selection, if proteins and chemical compounds can be directed into OMVs by the cell and secreted to the extracellular medium (Lappann et al., 2013; Elhenawy et al., 2014). In some bacteria, OMV

synthesis can be triggered under stress conditions, such as antibiotic treatments that activate SOS response and under oxidative stress (McBroom and Kuehn, 2007; Maredia et al., 2012; Macdonald and Kuehn, 2013; Schwechheimer and Kuehn, 2013). Under these situations, OMVs may serve as a way to remove potentially harmful compounds, such as misfolded proteins.

OMVs may promote the acquisition of nutrients and essential ions such as iron and zinc in bacterial communities and during host colonization (Evans et al., 2012; Toledo et al., 2012; Biller et al., 2014; Schwechheimer and Kuehn, 2015). The role of OMVs in nutrition has been suggested for different bacteria, such as *M. xanthus*, the cyanobacterium *Prochlorococcus* sp., *Borrelia burgdorferi*, *Neisseria meningitidis*, *Porphyromonas gingivalis*, *Moraxella catarrhalis*, and for cytoplasmic membrane vesicles of *Mycobacterium tuberculosis* (Aebi et al., 1996; Evans et al., 2012; Toledo et al., 2012; Lappann et al., 2013; Biller et al., 2014). It is not clear if OMVs have a universal role for nutrient acquisition, but in some cases they have been suggested to act as public goods that benefit the producer cells as well as other bacteria from the community that can absorb them or use the products released by the action of enzymes located in the OMVs (Evans et al., 2012; Elhenawy et al., 2014; Schwechheimer and Kuehn, 2015). An example is the relationship between bacteria found in the gut microbiota. OMVs produced by *Bacteroides* species carry hydrolases and polysaccharide lyases which can be used by bacteria that do not produce these enzymes to metabolize polysaccharides as nutrient sources in a mutualistic interaction (Rakoff-Nahoum et al., 2014).

Few studies have focused in the OMVs of phytopathogens. Still, research on this topic has revealed that, similarly to their animal-colonizing counterparts, bacteria that inflict diseases on plants were found to produce vesicles loaded with virulence-associated proteins and are capable of inducing immune responses on their hosts (Sidhu et al., 2008; Solé et al., 2015; Bahar

et al., 2016; Nascimento et al., 2016; Katsir and Bahar, 2017; Feitosa-Junior et al., 2019). These observations include *Xanthomonas* species and the closely related plant pathogen *Xylella fastidiosa*.

Strains from the genus *Xanthomonas*, known to cause diseases in a number of plant hosts, frequently contain most of the traditional bacterial macromolecular secretion systems named type I to VI (Büttner and Bonas, 2010; Alvarez-Martinez et al., 2021). OMVs, however, are comparatively much less studied than these other systems in these bacteria. Thus, this work focuses on unveiling the composition and possible roles of vesicles from one such phytopathogen, the causative agent of citrus canker disease, *Xanthomonas citri* pv. *citri* strain 306 (*X. citri*). Long extracellular appendages composed of OMVs were identified under different culture conditions, and the purified OMVs were investigated by elemental analysis, proteomic and lipidomic techniques, as well as by functional approaches. The vesicles were found to be potential vehicles of nutrients and essential ions available for incorporation by bacterial cells. This function, in association with the esterase and protease activities observed in the purified *X. citri* OMVs, may possibly aid in the microbial colonization of the plant host and contribute to disease establishment.

Results and Discussion

Visualization of X. citri *outer membrane vesicles and tubes by negative stain TEM*

Negative stain transmission electron microscopy (TEM) revealed the presence of tubular extensions from *X. citri* cells grown in plates of different culture media, identified as outer membrane tubes (**Fig. 1**). Upon closer inspection, the tubes were found to be formed from vesicle chains, occasionally with a well-defined segmentation but frequently presenting nearly

indistinguishable boundaries between links, seeming almost continuous. The size of the tubes ranged from short segments up to a few micrometers in length. Surrounding the cells in all conditions tested, a multitude of outer membrane vesicles (OMVs) was also present (**Fig. 1**). For most of their extension, the tubes appear to be composed of vesicles with a more homogeneous diameter (58-74 nm) than the isolated OMVs. Each tube seem to possess larger vesicles at its tips (88-103 nm), and some longer tubes appear to be formed by segments connected by these larger subunits.

Amongst the different culture media tested, Silva–Buddenhagen (SB) plates (Ou, 1985) seemingly produced the largest amount of tubes and vesicles, and thus were used for further experiments. The agar percentage (0.6 – 1.5%) seemed to not significantly affect the production of tubes, but these structures seemed to be rarer when the cells were grown in liquid medium (**Fig. S1**).

Purification of outer membrane vesicles combined with lipidomics and proteomics analyses

Pure, cell-free, OMVs could be purified from cultures grown in SB plates by filtration and density gradient centrifugation generating a clear yellow suspension (**Fig. 2A**). The tubes did not appear in the final preparations, being either lost during the process or disassembling from the manipulation (**Fig. 2B**). The purity of the OMV preparations was confirmed by negative stain TEM and absence of growth from contaminating cells. In addition to that, dynamic light scattering (DLS) was employed to measure their diameter distribution. The vesicles were determined to be monodispersed, with sizes ranging from about 40 to 150 nm, with a peak at around 75 nm (**Fig. 2C**), well within previous descriptions for OMVs (Schwechheimer and

Kuehn, 2015). The purified samples were then subjected to different analytical procedures to reveal their molecular composition.

Lipidomic analysis by liquid chromatography-tandem mass spectrometry (LC-MS/MS) of pure OMVs, partially purified OMV preparations ("OMV-enriched" samples, in which the cells were removed by filtration but not submitted to the density gradient centrifugation step), and whole *X. citri* cells revealed substantial differences between the samples. Sixty-six different lipids were identified, divided into 6 subclasses: cardiolipins (CL), free fatty acids (FFA), phosphatidylcholine (PC), phosphatidylethanolamine (PE), phosphatidylglycerol (PG), and methylated-phosphatidylserine (PS-Me) (**Fig. 3A**). CL, a type of diphosphatidylglycerol lipid, was the most diverse and abundant lipid subclass in all samples (**Fig. 3B**). The main difference observed was that, in relation to whole cells, pure OMVs appeared to be enriched in CL and relatively impoverished in PG (the biosynthetic precursor of CL). Free fatty acids were highly prevalent, likely reflecting their important role as common metabolic intermediates. It is important to note that the main components of the outer leaflet of bacterial outer membranes, lipopolysaccharides (LPS), were not evaluated in this analysis due to their relatively hydrophilic nature, making them too polar to be extracted along the other lipids.

A volcano plot analysis revealed 20 altered lipids between OMV-containing and whole cell samples, all presenting significant ($p<0.05$; FDR-adjusted t-test) fold changes values above 1.5 (**Fig. S2**). In the heatmap distribution for these altered lipids, according to one-way ANOVA, each sample type clustered with its replicates, with the OMVs (partially or completely purified) grouping separately from whole cells (**Fig. 3C**). Interestingly, it could be observed that the OMVs had relatively increased amounts of several CL species linked to saturated fatty acids and

206 decreased quantities of phospholipids (including CL) linked to unsaturated fatty acids when
207 compared to the whole cells.

208 The cone-shaped lipid CL is known to localize to negative curvature regions on
209 membranes (Renner and Weibel, 2011; Beltran-Heredia et al., 2019), such as in the inner leaflet
210 of *X. citri* OMVs, which present small diameters and are thus highly curved structures.
211 Additionally, the relatively higher saturation of the CL-linked chains in the vesicles may grant
212 the OMVs with more membrane rigidity (Tashiro et al., 2011). CL has been described as
213 organizing into microdomains where CL-interacting proteins localize (Sorice et al., 2009;
214 Planas-Iglesias et al., 2015; Lin and Weibel, 2016). In this manner, protein affinity for these
215 lipids could contribute cargo sorting into *X. citri* OMVs.

216 Nanoflow liquid chromatography-tandem mass spectrometry (nLC-MS/MS) was used for
217 the proteomic analysis of two replicates of purified OMV suspensions using in-solution
218 digestion. Parallel to that, four bands of OMV proteins separated in a SDS-PAGE gel were used
219 for a gel electrophoresis liquid chromatography (GeLC) approach using in-gel digestion (**Fig.**
220 **4A**). The data from the gel band samples were pooled and quantitatively compared to the two
221 replicates of the in-solution digestion. A total of 698 proteins were identified with at least one
222 peptide, with 561 proteins presenting two or more peptides (**Data Set S1** and **Data Set S2**).
223 Using their iBAQ (intensity based absolute quantification) values, the top 100 most abundant
224 proteins from each sample were selected and compared (**Fig. 4B**). While the in-solution
225 duplicates presented a large overlap, sharing 86 of their top 100 proteins, the GeLC approach
226 (gel bands samples) revealed the most distinct profile, with 49 of their most abundant proteins
227 being unique to its set.

The grouping of the top 100 non-redundant proteins with the highest iBAQ values for each sample yielded a list of 163 different proteins (**Table S1**). Subcellular localization prediction with PSORTb, manually curated based on sequence annotations, pointed out that 42.3% of these sequences are expected to be outer membrane proteins and 12.3% are likely periplasmic (**Fig. 5A**). The presence of inner membrane and cytoplasmic components observed in the proteome of *X. citri* OMVs, including ribosomal proteins, is commonly reported in the literature but remains unexplained as to how these proteins might associate to OMVs (Schwechheimer and Kuehn, 2015; Sjöström et al., 2015; Toyofuku et al., 2019; Zwarycz et al., 2020). Additionally, a cellular location could not be predicted for 21.5% of the identified proteins. For a different view on protein localization, SignalP was used to predict the secretion mechanisms of the OMV proteins (**Fig. 5B**). Nearly half of them (49.7%) contained signal peptides and almost one-fifth (19%) were predicted lipoproteins. A large "other" category (29.4%) includes cytoplasmic components and other proteins with non-classical or unknown secretion mechanisms.

From a functional perspective, proteins containing a TonB-dependent receptor domain were the most significantly enriched in the vesicles in comparison to the *X. citri* pv. *citri* 306 genome (**Fig. 5C**), as determined for Pfam annotations by the statistical enrichment analysis function of the STRING database (Franceschini et al., 2013). In accordance with that, the STRING analysis also identified a number of InterPro domains related to TonB-dependent receptors as the most significantly enriched in the samples (**Fig. S3**). In total, of the 163 most abundant proteins (**Table S1**), 31 were found to contain a "TonB-dependent receptor" Pfam domain (PF00593), the same set which contained a "TonB-dependent receptor-like, beta-barrel" InterPro domain (IPR000531). In a previous report, TonB-dependent receptors were found to

compose the majority of the identified outer membrane proteins in OMVs from *Xanthomonas campestris* pv. *campestris* (Sidhu et al., 2008). These outer membrane receptors are known to transport a range of nutrients, including metal-binding compounds (particularly siderophores), nickel complexes, vitamin B_{12}, and carbohydrates (Blanvillain et al., 2007; Krewulak and Vogel, 2011). Based on sequence annotations, the OMV proteome presents different types of TonB-dependent receptors which may bind diverse substrates (**Table S1**). These proteins are expected to remain able to bind to their specific ligands in the surface of the OMVs, though their internalization should not occur under these conditions since inner membrane components of this transport system are necessary to power substrate translocation (Krewulak and Vogel, 2011).

OMVs as sources of nutrients and essential metals

Based on similar observations in relation to ion transporters in their proteomes, OMVs from different bacterial species have been suggested to be involved in metal acquisition (Schwechheimer and Kuehn, 2015). Given this abundance of TonB-dependent receptors in the *X. citri* OMVs, mainly associated with siderophore transport, chrome azurol S (CAS) agar plates (Schwyn and Neilands, 1987) were used as a qualitative assay to evidence the presence of this type of molecule associated with the purified vesicles. OMV suspensions added to the medium caused its discoloration, indicating the displacement of the iron in the blue-colored CAS complex by the putative high affinity siderophores present in the samples (**Fig. 6A**). It is interesting to note that the iron-scavenging role of siderophores for microbial growth can also be important in phytopathogens for interactions with the host plant, promoting virulence and potentially triggering immune responses (Aznar and Dellagi, 2015).

To further investigate the association of the OMVs with essential metals, their elemental composition was determined by triple quadrupole inductively coupled plasma-mass spectrometry

(TQ ICP-MS) (**Fig. 6B**). **Table S2** presents the full results for all tested elements (C, Mg, S, Ca, Mn, Fe, Co, Ni, Cu, Zn, Br, Se, I, and Ba). The relative concentration of the elements in relation to carbon, reported as element-to-carbon ratios, was used as a comparative abundance value of the chemical elements in OMVs. The analysis confirmed the presence iron in the OMVs (899±450 ppb in relation to carbon), concurrent with the observed occurrence of receptors for iron-binding molecules in the vesicles and evidence for the presence of siderophores in the samples. Yet, iron was found at a smaller concentration than calcium (229±54 ppm) and magnesium (58±5 ppm), which are probably mostly bound to the LPS layer on the vesicles' surface (Coughlin et al., 1983), thus explaining their relative abundance. Zinc (9±5 ppm) was another biologically important metal ion determined at substantial levels in the OMVs. It can be used as a cofactor for different enzymes, including for metallopeptidases known to contribute to the pathogenicity of some organisms (Hase and Finkelstein, 1993). In fact, a few such zinc-dependent metallopeptidases were identified in the OMVs (**Data Set S1** and **Data Set S2**), though their specific biological roles have not yet been defined. In addition to that, manganese (450±45 ppb) can also act as a cofactor in a number of different enzymes and was also quantified in the samples. At last, cobalt (12±5 ppb) was detected in the vesicles. This is interesting given that among the TonB-dependent receptors enriched in the OMVs (**Table S1**), at least one is annotated as specific for vitamin B_{12}, a molecule which contains a coordinated cobalt ion. This protein, XAC3194, specifically contains a "TonB-dependent vitamin B_{12} transporter BtuB" InterPro Domain (IPR010101).

To test if the vesicles and the material associated to them are accessible to *X. citri* cells and can be utilized by them as nutrient sources, purified OMVs were tested as the sole carbon source for microbial growth. Substantial growth was observed for the samples where OMVs

were added, with the highest vesicle protein concentration tested leading to a multiplication of about 1000-fold in colony-forming units (**Fig. 6C**), indicating that the macromolecules associated with the vesicles were being consumed by the bacteria. This confirms the ability of these structures and the material they carry to be incorporated and used by cells, strengthening the hypothesis that they can act as nutrient vehicles such as has been proposed for other bacteria (Aebi et al., 1996; Evans et al., 2012; Toledo et al., 2012; Lappann et al., 2013; Biller et al., 2014; Schwechheimer and Kuehn, 2015). The mechanism for this incorporation, however, remains unclear. It could be mediated by the degradation of the vesicles for the release of their contents in some manner, but fusion of the OMVs to the cells' surfaces can also possibly be considered (Evans et al., 2012).

Esterase and protease activity of OMVs

Additional functional assays with the purified *X. citri* OMVs revealed they present esterase activity. Qualitative assays on agar plates evidenced their capacity to cause the hydrolysis of the triglyceride tributyrin emulsified in the medium, generating a clear halo (**Fig. 7A**), as well as to release the fatty acids from molecules of Tween 20, leading to their precipitation with the calcium added to the plates (**Fig. 7B**). Further assays were performed in suspension with *p*-nitrophenyl butyrate (*p*NP-C4) and *p*-nitrophenyl octanoate (*p*NP-C8) as chromogenic substrates, adding controlled amounts of vesicles quantified by their protein content. Using *p*NP-C4, a clear trend could be observed of increasing OMV protein concentration leading to faster product release (**Fig. 7C**). The longer chain substrate *p*NP-C8 was also hydrolyzed, but there were no clear differences between the different quantities of added vesicles (**Fig. 7D**). This is probably due to the low solubility of *p*NP-C8 in the medium, thus becoming the limiting factor for the reaction. Nonetheless, with both *p*-nitrophenyl esters, a

plateau seems to have been reached during the incubation with the OMVs, suggesting all the available substrate was consumed.

The esterase activity associated with the OMVs measured for a broad range of substrates can possibly be attributed to the outer membrane esterase with an autotransporter domain XAC3300 (gene name *estA*) identified among the most abundant proteins in the proteome, though other undetected enzymes may be present. Esterases have been reported to contribute to the virulence of phytopathogens, playing roles such as aiding in the degradation of cutin, pectin, or xylan in plant host tissues (Fett et al., 1992; Aparna et al., 2009; Tamir-Ariel et al., 2012; Dejean et al., 2013; Nascimento et al., 2016; Tayi et al., 2016; Ueda et al., 2018), depending on their substrate preference. In *Xanthomonas oryzae* pv. *oryzae*, loss of function of the LipA esterase lead to loss of virulence on rice and to the inability to induce host defense responses (Aparna et al., 2009), while a LipA mutant of *Xanthomonas campestris* pv. *vesicatoria* induced less severe symptoms on tomato than the wild type (Tamir-Ariel et al., 2012). The LipA ortholog of the related plant pathogen *Xylella fastidiosa*, LesA, was found to be present in OMVs. This esterase was able to induce hypersensitive response-like symptoms in grapevine leafs, while a LesA mutant showed decreased virulence (Nascimento et al., 2016). At last, a LipA mutant of *X. citri* presented reduced symptoms when inoculated into citrus leaves (Assis et al., 2017). This particular protein (XAC0501), however, could not be identified in the *X. citri* OMV proteome (**Data Set S1** and **Data Set S2**) but other esterases could perform similar functions in the plant host.

Proteases are another class of hydrolases that have been associated to pathogenesis in plant-infecting microorganisms (Hou et al., 2018; Figaj et al., 2019). In the *X. citri* OMV samples, this enzymatic activity was identified utilizing a fluorescent casein substrate (**Fig. 8**),

343 revealing yet another function connected to these structures. More substrate degradation was
344 observed with the addition of increasing amounts of OMVs to the reactions, while a commercial
345 EDTA-free protease inhibitor mix was able to substantially reduce activity (**Fig. 8**). In *X.*
346 *campestris* pv. *campestris*, a protease-deficient mutant presented a substantial loss of
347 pathogenicity in turnip leaves (Dow et al., 1990), whereas the XCV3671 protease of *X.*
348 *campestris* pv. *vesicatoria* was determined to contribute to virulence in pepper plants and
349 evidenced to be secreted in association with OMVs from this strain (Solé et al., 2015). Further
350 research could show if similar enzymes, both proteases and other esterases, are important for *X.*
351 *citri* infection and citrus canker development.

352 Considering the identified enzymatic activities associated with the *X. citri* OMVs, as well
353 as the presence of other hydrolases detected by proteomic analyses (**Table S1**), the vesicles may
354 be an important resource in plant colonization and pathogenesis. The release of products from
355 the degradation of macromolecules can be another manner in which the vesicles would be related
356 to nutrient acquisition, acting as public goods for other *X. citri* cells and possibly the microbial
357 community in general. These processes can facilitate the bacterial colonization of plant tissues
358 and thus participate in disease development.

359

360 **Conclusion**

361 *X. citri* cells express outer membrane tubes and vesicles carrying proteins, molecules, and
362 ions that may benefit bacterial cells. The OMV lipid profile revealed their higher content of
363 saturated cardiolipins with a relative impoverishment in unsaturated lipids. This might grant
364 them more rigidity while maintaining the small diameter of the vesicles. The proteome of the
365 vesicles revealed an abundance of transporters related to the uptake of nutrient molecules from

366 the medium. This includes receptors for siderophores, which were also potentially detected in the
367 samples as well as different biologically important metals. Based on these observations, our
368 hypothesis that the OMVs from *X. citri* can be used for sharing resources in microbial
369 communities is also supported by the observation that the vesicles' contents can be assimilated
370 and used for microbial growth. At last, another potential resource packaged with the OMVs is
371 their esterase and protease activities, which can release nutrients from the plant host tissue and
372 help to promote microbial colonization, potentially facilitating infection.

373 This work further establishes the association of OMVs with the acquisition and sharing of
374 nutrient molecules and ions in microbial communities. Microbial interactions can be important
375 driving forces shaping community structure in oligotrophic habitats such as leaf surfaces
376 (Schlechter et al., 2019). The balance between this apparently cooperative behavior with
377 *Xanthomonas*' notorious competitive proclivities conferred by its bactericidal type IV secretion
378 system (Sgro et al., 2019) may be especially significant for co-occurring epiphytic bacteria and
379 their own particular interactions with the plant (Hassani et al., 2018). Further research on this
380 possible indirect modulation of host physiology could reveal unexplored processes emerging
381 from a pathogen aptly manipulating microbial interaction networks with its diverse suite of
382 secretions systems.

383

384 **Materials and Methods**

385 *Bacterial cultures and growth conditions*

386 For all experiments, *Xanthomonas citri* pv. *citri* strain 306 (*X. citri*) was first grown in
387 liquid LB medium (tryptone, 10 g l^{-1}; yeast extract, 5 g l^{-1}; NaCl, 10 g l^{-1}) at 30 °C to OD 0.3 at
388 600 nm. The cultures were then inoculated on different solid culture media and incubated at 30

°C for 3 days. SB medium (yeast extract, 5 g l^{-1}; peptone, 5 g l^{-1}; glutamic acid, 1 g l^{-1}; sucrose, 5 g l^{-1}; pH 7) with 1.5% of agar (w/v) (Ou, 1985), was used for the production and purification of OMVs.

Purification of OMVs

X. citri colonies grown on SB plates at 30 °C for 3 days were scraped from the agar surfaces and suspended in phosphate buffered saline, PBS (NaCl, 8 g l^{-1}; KCl, 0.2 g l^{-1}; Na_2HPO_4, 1.44 g l^{-1}; KH_2PO_4, 0.24 g l^{-1}). After homogenization of the suspension, cells were precipitated by multiple centrifugations steps (10,000 - 30,000 × g at 4 °C, Beckman Avanti J-30I) until the supernatant appeared clean. Then, the samples were ultracentrifuged at 100,000 × g at 4 °C for at least 2 hours to pelletize the OMVs. The pellets were resuspended in a small volume of PBS and filtered through a 0.22 μm syringe filter to remove remaining cells inside a laminar flow hood. The samples were aseptically manipulated from this step on. The filtered OMVs were further purified by being loaded at the bottom of a filtered OptiPrep (Sigma) density gradient (35 to 0% in PBS) and ultracentrifuged at 200,000 × g for at least 12 hours at 4 °C (Beckman Optima XL-100K). The corresponding clear yellow band was collected, diluted in PBS, and pelletized again at 100,000 × g for 2 hours to wash out the density gradient medium. Absence of contamination was determined by lack of growth on LB plates incubated at 30 °C. DLS (Malvern Zetasizer) was used to characterize the size of the recovered OMVs. Total proteins in purified samples were quantified by a Qubit 3.0 fluorometer (Thermo Scientific).

Sodium dodecyl sulfate-polyacrylamide gel electrophoresis (SDS-PAGE)

Purified OMV samples were added with SDS-PAGE reducing sample buffer and treated at 90 °C for 10 minutes. Proteins were separated in 15% Tris-Glycine SDS-PAGE gels and stained with Coomassie Brilliant Blue.

Negative stain transmission electron microscopy (TEM)

Samples were applied to glow-discharged carbon film-coated copper grids (400 Mesh, CF400-Cu, Electron Microscopy Sciences), washed with Milli-Q ultrapure water, and negatively stained with uranyl acetate 2% (w/v), blotting on filter paper after each step. A FEI Tecnai G20 200 kV TEM (Department of Cell and Developmental Biology, Institute of Biomedical Sciences, University of São Paulo) or a JEOL JEM 2100 200 kV TEM (Institute of Chemistry, University of São Paulo) were used for image acquisition.

Liquid chromatography-tandem mass spectrometry lipidomics

Lipids were extracted by the Bligh and Dyer method (Bligh and Dyer, 1959), using ethanol-washed glass tubes and glass Pasteur pipettes for all steps. 100 µl of the samples were added to 400 µl of PBS (50 mM) containing 100 µM of deferoxamine. In the same tubes, 200 µl of a mix of internal standards (Avanti Polar Lipids and Sigma) and 300 µl of butylated hydroxytoluene (BHT) in methanol were added. The samples were then mixed with chloroform/ethyl acetate solution (4:1) and vortexed for 1 minute. Next, the tubes were centrifuged at 1,500 × g for 2 minutes at 4 °C and the organic phase at the bottom was collected and transferred to a clean vial. The solvent was dried under a flow of N_2 and the lipids were resuspended in 100 µl of isopropyl alcohol. The samples were stored at -80 °C before being analyzed by a previously established untargeted lipidomic method (Chaves-Filho et al., 2019).

Sample preparation for proteomics analysis

For in-solution digestion, OMV samples were boiled for 10 minutes before the proteins were precipitated with ethanol/acetone, and dissolved in urea 8 M in NH_4HCO_3 100 mM. Dithiothreitol (DTT) was added to a final concentration of 10 mM, and the samples were incubated for 30 min at 37 °C. The samples were cooled down, iodoacetamide was added to a

final concentration of 40 mM, and the samples were then incubated for 30 min at room temperature in the dark. DTT was added again, followed by digestion buffer (NH_4HCO_3 50 mM in a solution of 10% acetonitrile - ACN) to dilute ten times the urea concentration. Trypsin was added to digestion buffer for a final trypsin to protein ratio of 1:50, and the solution was incubated overnight at 37 °C. The digestion was stopped by the addition of formic acid (FA).

For in-gel digestion (GeLC approach), the gel bands were completely destained, treated with 10 mM DTT at 56 °C for 45 min, 55 mM IAA at room temperature for 30 min in the dark and digested at 37 °C for 16 hrs with 2 µg sequencing grade modified trypsin, Porcine (Promega). The resultant peptides were extracted in 40% ACN/0.1% TFA into fresh Protein LoBind® microtubes, dried down by vacuum centrifugation, and resuspended in 50 µL 0.1% TFA. Peptide samples obtained from the in-solution and in-gel digestions were desalted using C18 disks packed in a p200 pipette tip. Peptides were eluted with 50% ACN and dried down.

Nano-flow liquid chromatography-tandem mass spectrometry-based proteomics

Tryptic peptides were resuspended in 0.1% FA and analyzed using an EASY-nLC system (Thermo Scientific) coupled to LTQ-Orbitrap Velos mass spectrometer (Thermo Scientific) at the Core Facility for Scientific Research at the University of São Paulo (CEFAP-USP/BIOMASS). The peptides were loaded onto a C18 PicoFrit column (C18 PepMap, 75 µm id × 10 cm, 3.5 µm particle size, 100 Å pore size; New Objective, Ringoes, NJ, USA) and separated with a gradient from 100% mobile phase A (0.1% FA) to 34% phase B (0.1% FA, 95% ACN) during 60 min, 34%–95% in 15 min, and 5 min at 95% phase B at a constant flow rate of 250 nL/min. The LTQ-Orbitrap Velos was operated in positive ion mode with data-dependent acquisition. The full scan was obtained in the Orbitrap with an automatic gain control target value of 10^6 ions and a maximum fill time of 500 ms. Each precursor ion scan was acquired at a

458 resolution of 60,000 FWHM in the 400–1500 m/z mass range. Peptide ions were fragmented by
459 CID MS/MS using a normalized collision energy of 35%. The 20 most abundant peptide were
460 selected for MS/MS and dynamically excluded for a duration of 30s. All raw data were accessed
461 in the Xcalibur software (Thermo Scientific).

462 *Proteomics data analysis*

463 Raw data were processed with MaxQuant (Tyanova et al., 2016) using Andromeda search
464 engine against the SwissProt *Xanthomonas axonopodis* pv. *citri* (strain 306) database (4354
465 entries downloaded from UniProt.org, Jan/2021) with common contaminants for protein
466 identification. Database searches were performed with the following parameters: precursor mass
467 tolerance of 10 ppm, product ion mass tolerance of 0.6 Da; trypsin cleavage with two missed
468 cleavage allowed; carbamidomethylation of cysteine (57.021 Da) was set as a fixed modification,
469 and oxidation of methionine (15.994 Da) and protein N-terminal acetylation (42.010 Da) were
470 selected as variable modifications. All identifications were filtered to achieve a protein peptide
471 and PSMs, false discovery rate (FDR) of less than 1%, and a minimum of one unique peptide
472 was required for protein identification. Protein quantification was based on the MaxQuant label-
473 free algorithm using both unique and razor peptides for protein quantification. Protein abundance
474 was assessed on label-free protein quantification (LFQ) based on extracted ion chromatogram
475 area of the precursor ions activating the matching between run features. Intensity based absolute
476 quantification (iBAQ) values were used to calculate the relative protein abundance within
477 samples. MS data have been submitted to the PRIDE repository, project accession: PXD025405,
478 username: reviewer_pxd025405@ebi.ac.uk, password: MyMyVfmr.

479 Statistical enrichment analyses of Pfam and InterPro domains and FDR calculations were
480 obtained from the STRING database (Franceschini et al., 2013). PSORTb 3.0 was used for

subcellular localization prediction of the identified proteins (Yu et al., 2010), followed by manual curation based on sequence annotations, and SignalP 5.0 was used for predicting protein secretion mechanisms (Armenteros et al., 2019).

Elemental analysis by Triple Quadrupole Inductively Coupled Plasma-Mass Spectrometry

Triple Quadrupole Inductively Coupled Plasma-Mass Spectrometry (iCAP TQ ICP-MS, Thermo Fisher Scientific, Bremen, Germany) equipped with a Micro Mist nebulizer (400 µL min^{-1}) combined with a cyclonic spray chamber (both obtained from ESI Elemental Service & Instruments GmbH, Mainz, Germany) and an auto-sampler ASX-560 (Teledyne CETAC Technologies, Omaha, NE, USA) was used to perform quantitative analysis of the elements in OMVs samples. The instrument was tuned prior to the elemental analysis to obtain the highest sensitivity. The interface was assembled using a nickel sample cone and a nickel skimmer cone with an insert version for high matrix (3.5 mm).

The TQ ICP-MS was operated with 99.999% Argon (Air Products). Helium and oxygen (99.999%, Linde) were used in the collision/reaction cell of the instrument. A screening (survey scan) was performed on the OMV samples and the PBS buffer (method blank) to identify the main chemical elements contained in the sample, recording the full mass spectrum from 4.6 to 245.0 u.. All measurements were performed in triplicate (n=3) according to selected masses showed in **Table S3.** All data were evaluated with Qtegra ISDS software (Thermo Scientific).

Mono-elemental standard solutions were used for calibration curves. Ca, Mn, Fe, Co, Ni, Cu, Zn, and Ba solutions (PlasmaCAL, SCP Science containing 1000 mg l^{-1} each) were used to calibrate these elements. Mg (1000 mg l^{-1}, CertiPUR, Merck), Se (1000 mg l^{-1}, Wako Pure Chemical Industries), oxalate standard for carbon quantification (10000 mg l^{-1}, TraceCERT,

Sigma-Aldrich), and Certified Multielement Ion Chromatography Anion Standard Solution for Bromine and Sulfur quantification (10 mg l^{-1}, TraceCERT, Sigma-Aldrich) were also used to calibrate these respectively elements. The OMV samples were diluted to 500 µl with PBS buffer prior to TQ ICP-MS analysis and PBS was used as a method blank. **Table S4** displays the main analytical performance characteristics achieved: linear range, sensitivity, limit of detection (LOD), and coefficient of determination.

Instrumental precision was checked by stability tests throughout the analysis (obtaining a relative standard deviation of less than 3% for all analytes) and the accuracy was checked by spike and recovery tests at four different levels of concentration, obtaining acceptable values ranging from 93 to 105%.

Siderophore detection and bacterial growth assays

The presence of siderophores in the purified OMVs was tested on chrome azurol S (CAS) agar plates (Schwyn and Neilands, 1987), prepared according to Louden et al. (2011). Bacterial growth using purified OMVs as sole carbon sources was assayed in M9 minimal medium without glucose (Na_2HPO_4, 6.8 g l^{-1}; KH_2PO_4, 3 g l^{-1}; NH_4Cl, 1 g l^{-1}; NaCl, 0.5 g l^{-1}; $MgSO_4$, 2 mM; $CaCl_2$, 2 mM). About 10^3 stationary phase cells l^{-1}, equivalent to around 10 colony forming units (CFU) for each 10 µl droplet plated, were used as the initial population for the experiments. To the samples, 0, 125, or 375 µg ml^{-1} of total OMV proteins were added, and the tubes were incubated at 30 °C in a thermomixer for 48 h. Aliquots were taken at regular intervals and plated in LB medium for CFU quantification.

Esterase activity assays

Esterase qualitative assays were performed on either LB plates prepared with 0.5% tributyrin emulsified by sonication (SONICS Vibra-Cell), or NYG plates (peptone, 5 g l^{-1}; yeast

527 extract, 5 g l^{-1}; glycerol, 20 g l^{-1}, agar, 1% (Turner et al., 1984)) containing 1% of Tween 20 and
528 4 mM of $CaCl_2$ (Ramnath et al., 2017). Esterase enzymatic activity was measured
529 colorimetrically with a reaction mixture (100 mM Tris-HCl pH 7.5, 50 mM NaCl) containing
530 500 µM of *p*NP-C4 or 200 µM of *p*NP-C8 with the addition of 10, 20, or 50 µg ml^{-1} of total
531 proteins of purified OMVs in microplate wells. The reactions were incubated at 30 °C and their
532 absorbance at 400 nm was measured with a SpectraMax Paradigm microplate reader (Molecular
533 Devices) at regular intervals of time during 4 h.

534 *Protease activity assays*

535 Protease assays were performed with a protease fluorescent detection kit using casein
536 labeled with fluorescein isothiocyanate (FITC) as the substrate following the manufacturer's
537 instructions (PF0100, Sigma-Aldrich). Briefly, 10 µl of the test samples were added to 40 µl of
538 FITC-casein in incubation buffer and incubated at 30 °C for 6 hours. PBS was used as a blank,
539 and the reactions contained 100, 200, or 300 µg ml^{-1} of total proteins of purified OMVs. For
540 some assays, EDTA-free Pierce Protease Inhibitor (A32965, Thermo Scientific) was added to
541 300 µg ml^{-1} samples to a final concentration equivalent to the manufacturer's recommendations
542 (1 tablet for 50 ml of solution). After incubation, undigested substrate was precipitated with the
543 addition of 150 µl of trichloroacetic acid 0.6 N for 30 min at 37 °C. Aliquots of the supernatants
544 containing FITC-labeled fragments were diluted in assay buffer and analyzed in a black 96-well
545 microplate with a SpectraMax Paradigm microplate reader (Molecular Devices). Relative
546 fluorescence units (RFU) were measured with excitation at 485 nm and detection at 535 nm. All
547 samples presented RFU measurements substantially above 120% of the value obtained with the
548 blank (data not shown), which is considered significant according to the kit's manufacturer.
549

Acknowledgements

The authors would like to thank Roberto Cabado Modia Junior and Alfredo Duarte for the technical assistance at the electron microscopy facilities, Thais Viggiani Santana for the assistance at the proteomics facility, and Tania Geraldine Churasacari Vinces for the assistance with the esterase activity experiments.

We thank the Core Facility for Scientific Research – University of São Paulo (CEFAP-USP/BIOMASS) for the proteomic analysis. The authors acknowledge financial support from the São Paulo Research Foundation (FAPESP): grants 2019/00195-2 and 2020/04680-0 to CRG, 2017/17303-7 to CSF, 2014/06863-3, 2018/18257-1 and 2018/15549-1 to GP, 2013/07937-8 to SM, 2016/09047-8 to RFdS, 2017/20752-8 to the EMU TQ ICP-MS facility at IPT, and scholarships 2018/21076-9 to GGA, 2017/24301-0 to MMC, 2017/10611-8 to ADP, 2019/12234-2 to EEL, and 2017/13804-1 to AI. The authors also acknowledge financial support from the Coordenação de Aperfeiçoamento de Pessoal de Nível Superior (CAPES) in the form of scholarships to MMY, IT, and GGA (88887.336498/2019-00), and the Brazilian National Council for Scientific and Technological Development (CNPq) for RP grants 380490/2018-8 and 380939/2020-7.

References

Aebi, C., Stone, B., Beucher, M., Cope, L.D., Maciver, I., Thomas, S.E. et al. (1996) Expression of the CopB outer membrane protein by Moraxella catarrhalis is regulated by iron and affects iron acquisition from transferrin and lactoferrin. *Infect Immun* **64**: 2024-2030.

571 Alvarez-Martinez, C.E., Sgro, G.G., Araujo, G.G., Paiva, M.R.N., Matsuyama, B.Y., Guzzo,
572 C.R. et al. (2021) Secrete or perish: The role of secretion systems in Xanthomonas biology.
573 *Computational and Structural Biotechnology Journal* **19**: 279-302.
574 Aparna, G., Chatterjee, A., Sonti, R.V., and Sankaranarayanan, R. (2009) A Cell Wall–
575 Degrading Esterase of *Xanthomonas oryzae* Requires a Unique Substrate Recognition Module
576 for Pathogenesis on Rice. *The Plant Cell* **21**: 1860-1873.
577 Armenteros, J.J.A., Tsirigos, K.D., Sonderby, C.K., Petersen, T.N., Winther, O., Brunak, S. et al.
578 (2019) SignalP 5.0 improves signal peptide predictions using deep neural networks. *Nature*
579 *Biotechnology* **37**: 420-+.
580 Assis, R.D.B., Polloni, L.C., Patane, J.S.L., Thakur, S., Felestrino, E.B., Diaz-Caballero, J. et al.
581 (2017) Identification and analysis of seven effector protein families with different adaptive and
582 evolutionary histories in plant-associated members of the Xanthomonadaceae. *Scientific Reports*
583 **7**.
584 Aznar, A., and Dellagi, A. (2015) New insights into the role of siderophores as triggers of plant
585 immunity: what can we learn from animals? *Journal of Experimental Botany* **66**: 3001-3010.
586 Bahar, O., Mordukhovich, G., Luu, D.D., Schwessinger, B., Daudi, A., Jehle, A.K. et al. (2016)
587 Bacterial Outer Membrane Vesicles Induce Plant Immune Responses. *Molecular Plant-Microbe*
588 *Interactions* **29**: 374-384.
589 Beltran-Heredia, E., Tsai, F.C., Salinas-Almaguer, S., Cao, F.J., Bassereau, P., and Monroy, F.
590 (2019) Membrane curvature induces cardiolipin sorting. *Communications Biology* **2**.
591 Biller, S.J., Schubotz, F., Roggensack, S.E., Thompson, A.W., Summons, R.E., and Chisholm,
592 S.W. (2014) Bacterial vesicles in marine ecosystems. *Science* **343**: 183-186.

593 Blanvillain, S., Meyer, D., Boulanger, A., Lautier, M., Guynet, C., Denance, N. et al. (2007)
594 Plant Carbohydrate Scavenging through TonB-Dependent Receptors: A Feature Shared by
595 Phytopathogenic and Aquatic Bacteria. *Plos One* **2**.
596 Bligh, E.G., and Dyer, W.J. (1959) A Rapid Method of Total Lipid Extraction and Purification.
597 *Canadian Journal of Biochemistry and Physiology* **37**: 911-917.
598 Büttner, D., and Bonas, U. (2010) Regulation and secretion of Xanthomonas virulence factors.
599 *Fems Microbiology Reviews* **34**: 107-133.
600 Cao, P., and Wall, D. (2019) Direct visualization of a molecular handshake that governs kin
601 recognition and tissue formation in myxobacteria. *Nature Communications* **10**: 3073.
602 Chaves-Filho, A.B., Pinto, I.F.D., Dantas, L.S., Xavier, A.M., Inague, A., Faria, R.L. et al.
603 (2019) Alterations in lipid metabolism of spinal cord linked to amyotrophic lateral sclerosis.
604 *Scientific Reports* **9**: 11642.
605 Coughlin, R.T., Tonsager, S., and Mcgroarty, E.J. (1983) Quantitation of Metal-Cations Bound
606 to Membranes and Extracted Lipopolysaccharide of Escherichia-Coli. *Biochemistry* **22**: 2002-
607 2007.
608 Dejean, G., Blanvillain-Baufume, S., Boulanger, A., Darrasse, A., de Bernonville, T.D., Girard,
609 A.L. et al. (2013) The xylan utilization system of the plant pathogen Xanthomonas campestris pv
610 campestris controls epiphytic life and reveals common features with oligotrophic bacteria and
611 animal gut symbionts. *New Phytologist* **198**: 899-915.
612 Dey, A., and Wall, D. (2014) A Genetic Screen in Myxococcus xanthus Identifies Mutants That
613 Uncouple Outer Membrane Exchange from a Downstream Cellular Response. *Journal of*
614 *Bacteriology* **196**: 4324-4332.

615 Dow, J.M., Clarke, B.R., Milligan, D.E., Tang, J.L., and Daniels, M.J. (1990) Extracellular
616 Proteases from *Xanthomonas campestris* pv. Campestris, the Black Rot Pathogen. *Applied and*
617 *Environmental Microbiology* **56**: 2994-2998.
618 Elhenawy, W., Debelyy, M.O., and Feldman, M.F. (2014) Preferential Packing of Acidic
619 Glycosidases and Proteases into Bacteroides Outer Membrane Vesicles. *Mbio* **5**.
620 Evans, A.G.L., Davey, H.M., Cookson, A., Currinn, H., Cooke-Fox, G., Stanczyk, P.J., and
621 Whitworth, D.E. (2012) Predatory activity of Myxococcus xanthus outer-membrane vesicles and
622 properties of their hydrolase cargo. *Microbiology* **158**: 2742-2752.
623 Feitosa-Junior, O.R., Stefanello, E., Zaini, P.A., Nascimento, R., Pierry, P.M., Dandekar, A.M. et
624 al. (2019) Proteomic and Metabolomic Analyses of Xylella fastidiosa OMV-Enriched Fractions
625 Reveal Association with Virulence Factors and Signaling Molecules of the DSF Family.
626 *Phytopathology* **109**: 1344-1353.
627 Fett, W.F., Gerard, H.C., Moreau, R.A., Osman, S.F., and Jones, L.E. (1992) Screening of
628 Nonfilamentous Bacteria for Production of Cutin-Degrading Enzymes. *Applied and*
629 *Environmental Microbiology* **58**: 2123-2130.
630 Figaj, D., Ambroziak, P., Przepiora, T., and Skorko-Glonek, J. (2019) The Role of Proteases in
631 the Virulence of Plant Pathogenic Bacteria. *International Journal of Molecular Sciences* **20**.
632 Fischer, T., Schorb, M., Reintjes, G., Kolovou, A., Santarella-Mellwig, R., Markert, S. et al.
633 (2019) Biopearling of Interconnected Outer Membrane Vesicle Chains by a Marine
634 Flavobacterium. *Applied and Environmental Microbiology* **85**: e00829-00819.
635 Franceschini, A., Szklarczyk, D., Frankild, S., Kuhn, M., Simonovic, M., Roth, A. et al. (2013)
636 STRING v9.1: protein-protein interaction networks, with increased coverage and integration.
637 *Nucleic Acids Research* **41**: D808-D815.

638 Guerrero-Mandujano, A., Hernandez-Cortez, C., Ibarra, J.A., and Castro-Escarpulli, G. (2017)
639 The outer membrane vesicles: Secretion system type zero. *Traffic* **18**: 425-432.
640 Hampton, C.M., Guerrero-Ferreira, R.C., Storms, R.E., Taylor, J.V., Yi, H., Gulig, P.A., and
641 Wright, E.R. (2017) The Opportunistic Pathogen Vibrio vulnificus Produces Outer Membrane
642 Vesicles in a Spatially Distinct Manner Related to Capsular Polysaccharide. *Frontiers in*
643 *Microbiology* **8**.
644 Hase, C.C., and Finkelstein, R.A. (1993) Bacterial Extracellular Zinc-Containing
645 Metalloproteases. *Microbiological Reviews* **57**: 823-837.
646 Hassani, M.A., Duran, P., and Hacquard, S. (2018) Microbial interactions within the plant
647 holobiont. *Microbiome* **6**.
648 Hellman, J., Loiselle, P.M., Zanzot, E.M., Allaire, J.E., Tehan, M.M., Boyle, L.A. et al. (2000)
649 Release of gram-negative outer-membrane proteins into human serum and septic rat blood and
650 their interactions with immunoglobulin in antiserum to Escherichia coli J5. *J Infect Dis* **181**:
651 1034-1043.
652 Hickey, C.A., Kuhn, K.A., Donermeyer, D.L., Porter, N.T., Jin, C., Cameron, E.A. et al. (2015)
653 Colitogenic Bacteroides thetaiotaomicron Antigens Access Host Immune Cells in a Sulfatase-
654 Dependent Manner via Outer Membrane Vesicles. *Cell Host Microbe* **17**: 672-680.
655 Hou, S.G., Jamieson, P., and He, P. (2018) The cloak, dagger, and shield: proteases in plant-
656 pathogen interactions. *Biochemical Journal* **475**: 2491-2509.
657 Katsir, L., and Bahar, O. (2017) Bacterial outer membrane vesicles at the plant-pathogen
658 interface. *Plos Pathogens* **13**.

659 Kim, Y.R., Kim, B.U., Kim, S.Y., Kim, C.M., Na, H.S., Koh, J.T. et al. (2010) Outer membrane
660 vesicles of Vibrio vulnificus deliver cytolysin-hemolysin Vvha into epithelial cells to induce
661 cytotoxicity. *Biochemical and Biophysical Research Communications* **399**: 607-612.
662 Krewulak, K.D., and Vogel, H.J. (2011) TonB or not TonB: is that the question? *Biochemistry*
663 *and Cell Biology* **89**: 87-97.
664 Lappann, M., Otto, A., Becher, D., and Vogel, U. (2013) Comparative proteome analysis of
665 spontaneous outer membrane vesicles and purified outer membranes of Neisseria meningitidis. *J*
666 *Bacteriol* **195**: 4425-4435.
667 Lin, T.Y., and Weibel, D.B. (2016) Organization and function of anionic phospholipids in
668 bacteria. *Applied Microbiology and Biotechnology* **100**: 4255-4267.
669 Louden, B.C., Haarmann, D., and Lynne, A.M. (2011) Use of Blue Agar CAS Assay for
670 Siderophore Detection. *Journal of Microbiology & Biology Education* **12**: 51-53.
671 Macdonald, I.A., and Kuehn, M.J. (2013) Stress-induced outer membrane vesicle production by
672 Pseudomonas aeruginosa. *J Bacteriol* **195**: 2971-2981.
673 Maredia, R., Devineni, N., Lentz, P., Dallo, S.F., Yu, J., Guentzel, N. et al. (2012) Vesiculation
674 from Pseudomonas aeruginosa under SOS. *ScientificWorldJournal* **2012**: 402919.
675 McBroom, A.J., and Kuehn, M.J. (2007) Release of outer membrane vesicles by Gram-negative
676 bacteria is a novel envelope stress response. *Mol Microbiol* **63**: 545-558.
677 McCaig, W.D., Koller, A., and Thanassi, D.G. (2013) Production of Outer Membrane Vesicles
678 and Outer Membrane Tubes by Francisella novicida. *Journal of Bacteriology* **195**: 1120-1132.
679 Nascimento, R., Gouran, H., Chakraborty, S., Gillespie, H.W., Almeida-Souza, H.O., Tu, A. et
680 al. (2016) The Type II Secreted Lipase/Esterase LesA is a Key Virulence Factor Required for
681 Xylella fastidiosa Pathogenesis in Grapevines. *Scientific Reports* **6**.

682 Ou, S.H. (1985) Bacterial leaf blight. In *Rice Diseases*: Commonwealth Mycological Institute,
683 pp. 61-96.
684 Pirbadian, S., Barchinger, S.E., Leung, K.M., Byun, H.S., Jangir, Y., Bouhenni, R.A. et al.
685 (2014) Shewanella oneidensis MR-1 nanowires are outer membrane and periplasmic extensions
686 of the extracellular electron transport components. *Proceedings of the National Academy of*
687 *Sciences of the United States of America* **111**: 12883-12888.
688 Pirbadian, S., Barchinger, S.E., Leung, K.M., Byun, H.S., Jangir, Y., Bouhenni, R.A. et al.
689 (2015) Bacterial Nanowires of Shewanella Oneidensis MR-1 are Outer Membrane and
690 Periplasmic Extensions of the Extracellular Electron Transport Components. *Biophysical Journal*
691 **108**: 368a-368a.
692 Planas-Iglesias, J., Dwarakanath, H., Mohammadyani, D., Yanamala, N., Kagan, V.E., and
693 Klein-Seetharaman, J. (2015) Cardiolipin Interactions with Proteins. *Biophysical Journal* **109**:
694 1282-1294.
695 Rakoff-Nahoum, S., Coyne, M.J., and Comstock, L.E. (2014) An ecological network of
696 polysaccharide utilization among human intestinal symbionts. *Curr Biol* **24**: 40-49.
697 Ramnath, L., Sithole, B., and Govinden, R. (2017) Identification of lipolytic enzymes isolated
698 from bacteria indigenous to Eucalyptus wood species for application in the pulping industry.
699 *Biotechnology Reports* **15**: 114-124.
700 Remis, J.P., Wei, D.G., Gorur, A., Zemla, M., Haraga, J., Allen, S. et al. (2014) Bacterial social
701 networks: structure and composition of Myxococcus xanthus outer membrane vesicle chains.
702 *Environmental Microbiology* **16**: 598-610.

703 Renner, L.D., and Weibel, D.B. (2011) Cardiolipin microdomains localize to negatively curved
704 regions of Escherichia coli membranes. *Proceedings of the National Academy of Sciences of the*
705 *United States of America* **108**: 6264-6269.
706 Sampath, V., McCaig, W.D., and Thanassi, D.G. (2018) Amino acid deprivation and central
707 carbon metabolism regulate the production of outer membrane vesicles and tubes by Francisella.
708 *Molecular Microbiology* **107**: 523-541.
709 Schlechter, R.O., Miebach, M., and Remus-Emsermann, M.N.P. (2019) Driving factors of
710 epiphytic bacterial communities: A review. *Journal of Advanced Research* **19**: 57-65.
711 Schwechheimer, C., and Kuehn, M.J. (2013) Synthetic effect between envelope stress and lack
712 of outer membrane vesicle production in Escherichia coli. *J Bacteriol* **195**: 4161-4173.
713 Schwechheimer, C., and Kuehn, M.J. (2015) Outer-membrane vesicles from Gram-negative
714 bacteria: biogenesis and functions. *Nature Reviews Microbiology* **13**: 605-619.
715 Schwyn, B., and Neilands, J.B. (1987) Universal Chemical-Assay for the Detection and
716 Determination of Siderophores. *Analytical Biochemistry* **160**: 47-56.
717 Sgro, G.G., Oka, G.U., Souza, D.P., Cenens, W., Bayer-Santos, E., Matsuyama, B.Y. et al.
718 (2019) Bacteria-Killing Type IV Secretion Systems. *Frontiers in Microbiology* **10**.
719 Shetty, A., Chen, S.C., Tocheva, E.I., Jensen, G.J., and Hickey, W.J. (2011) Nanopods: A New
720 Bacterial Structure and Mechanism for Deployment of Outer Membrane Vesicles. *Plos One* **6**.
721 Sidhu, V.K., Vorholter, F.J., Niehaus, K., and Watt, S.A. (2008) Analysis of outer membrane
722 vesicle associated proteins isolated from the plant pathogenic bacterium Xanthomonas
723 campestris pv. campestris. *Bmc Microbiology* **8**.
724 Sjöström, A.E., Sandblad, L., Uhlin, B.E., and Wai, S.N. (2015) Membrane vesicle-mediated
725 release of bacterial RNA. *Scientific Reports* **5**.

726 Solé, M., Scheibner, F., Hoffmeister, A.K., Hartmann, N., Hause, G., Rother, A. et al. (2015)
727 Xanthomonas campestris pv. vesicatoria Secretes Proteases and Xylanases via the Xps Type II
728 Secretion System and Outer Membrane Vesicles. *Journal of Bacteriology* **197**: 2879-2893.
729 Sorice, M., Manganelli, V., Matarrese, P., Tinari, A., Misasi, R., Malorni, W., and Garofalo, T.
730 (2009) Cardiolipin-enriched raft-like microdomains are essential activating platforms for
731 apoptotic signals on mitochondria. *Febs Letters* **583**: 2447-2450.
732 Tamir-Ariel, D., Rosenberg, T., Navon, N., and Burdman, S. (2012) A secreted lipolytic enzyme
733 from Xanthomonas campestris pv. vesicatoria is expressed in planta and contributes to its
734 virulence. *Molecular Plant Pathology* **13**: 556-567.
735 Tashiro, Y., Inagaki, A., Shimizu, M., Ichikawa, S., Takaya, N., Nakajima-Kambe, T. et al.
736 (2011) Characterization of Phospholipids in Membrane Vesicles Derived from Pseudomonas
737 aeruginosa. *Bioscience Biotechnology and Biochemistry* **75**: 605-607.
738 Tayi, L., Maku, R.V., Patel, H.K., and Sonti, R.V. (2016) Identification of Pectin Degrading
739 Enzymes Secreted by Xanthomonas oryzae pv. oryzae and Determination of Their Role in
740 Virulence on Rice. *Plos One* **11**.
741 Toledo, A., Coleman, J.L., Kuhlow, C.J., Crowley, J.T., and Benach, J.L. (2012) The enolase of
742 Borrelia burgdorferi is a plasminogen receptor released in outer membrane vesicles. *Infect*
743 *Immun* **80**: 359-368.
744 Toyofuku, M., Nomura, N., and Eberl, L. (2019) Types and origins of bacterial membrane
745 vesicles. *Nature Reviews Microbiology* **17**: 13-24.
746 Turner, P., Barber, C., and Daniels, M. (1984) Behavior of the Transposons Tn5 and Tn7 in
747 Xanthomonas-Campestris Pv Campestris. *Molecular & General Genetics* **195**: 101-107.

748 Tyanova, S., Temu, T., and Cox, J. (2016) The MaxQuant computational platform for mass
749 spectrometry-based shotgun proteomics. *Nature Protocols* **11**: 2301-2319.
750 Ueda, H., Kurose, D., Kugimiya, S., Mitsuhara, I., Yoshida, S., Tabata, J. et al. (2018) Disease
751 severity enhancement by an esterase from non-phytopathogenic yeast Pseudozyma antarctica and
752 its potential as adjuvant for biocontrol agents. *Scientific Reports* **8**.
753 Yu, N.Y., Wagner, J.R., Laird, M.R., Melli, G., Rey, S., Lo, R. et al. (2010) PSORTb 3.0:
754 improved protein subcellular localization prediction with refined localization subcategories and
755 predictive capabilities for all prokaryotes. *Bioinformatics* **26**: 1608-1615.
756 Zwarycz, A.S., Livingstone, P.G., and Whitworth, D.E. (2020) Within-species variation in OMV
757 cargo proteins: the Myxococcus xanthus OMV pan-proteome. *Molecular Omics* **16**: 387-397.
758

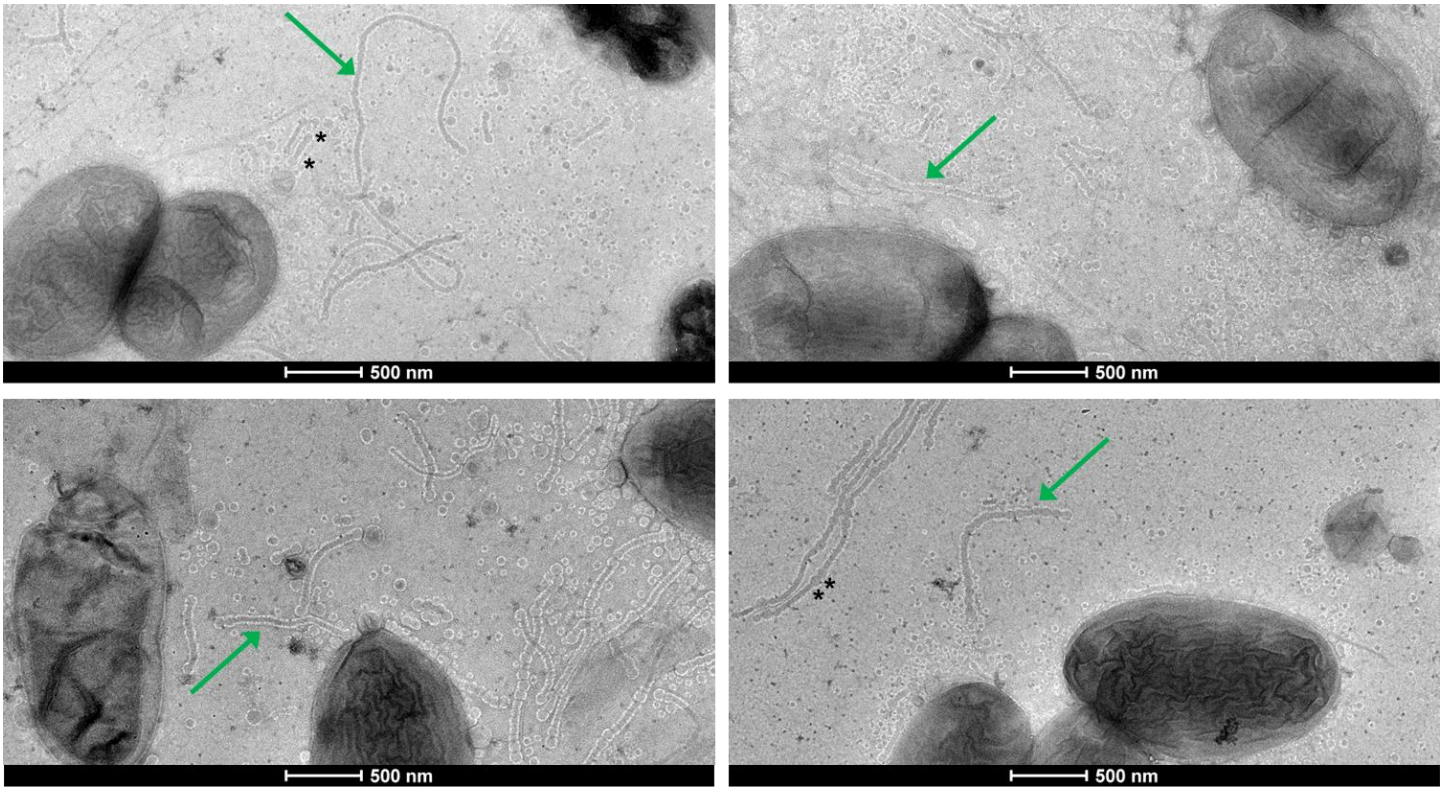

759

760 **Fig. 1.** Outer membrane tubes and vesicles from *X. citri*. Cells were grown in SB with
761 agar 0.6% and imaged by negative stain TEM. The green arrows point to examples of the outer
762 membrane tubes that can be seen in the images. Asterisks (*) indicate some occurrences of larger
763 vesicles at the tips or within tubes.

764

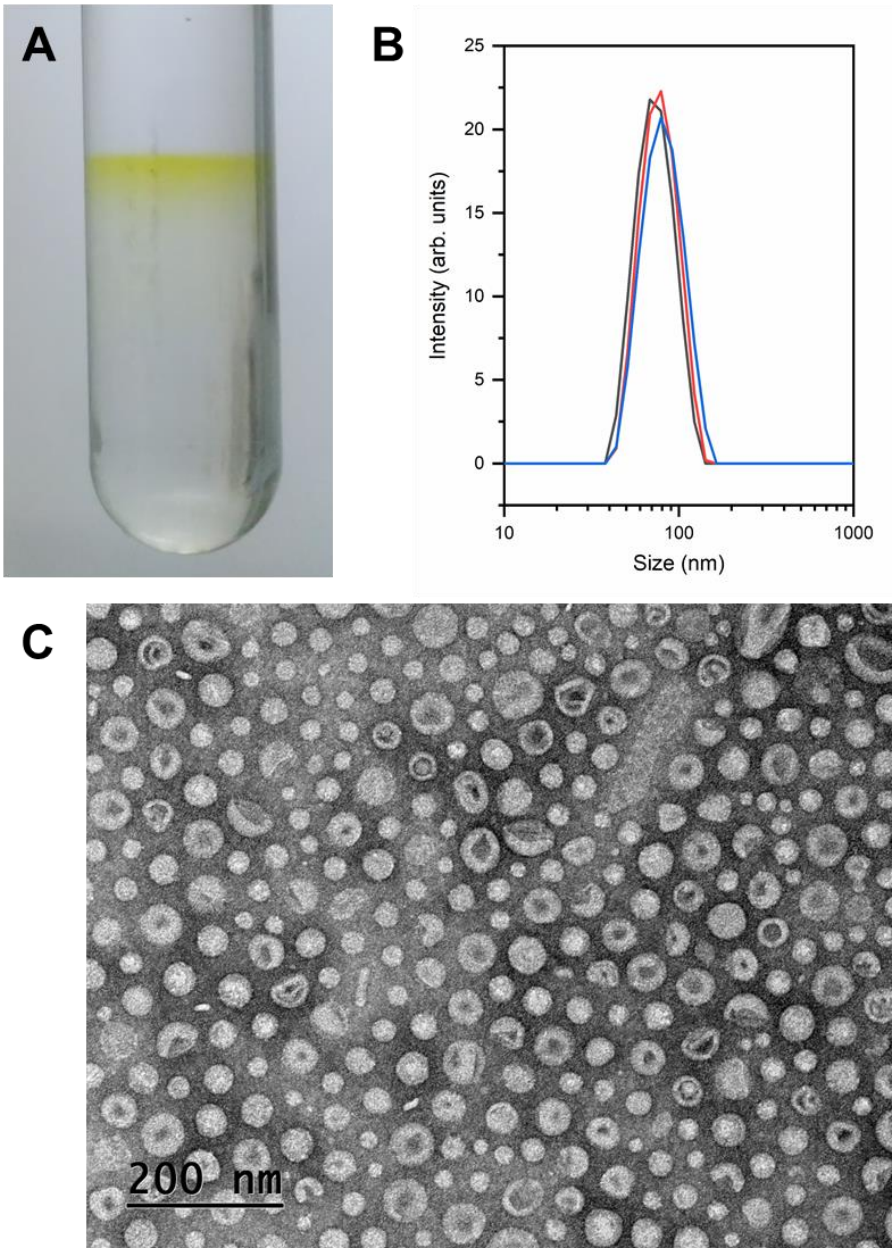

765

766 **Fig. 2.** Purification and characterization of the *X. citri* outer membrane vesicles (OMVs).
767 Vesicles were retrieved as a yellow band from the density gradient centrifugation tubes (A). The
768 vesicle size distribution was determined by DLS and observed to range from about 40 to 150 nm
769 in diameter, with a peak near 75 nm (B). Observation by negative stain TEM confirmed the
770 purification of the OMVs, allowing the evaluation of their size, morphology, and lack of
771 contaminating cells (C).

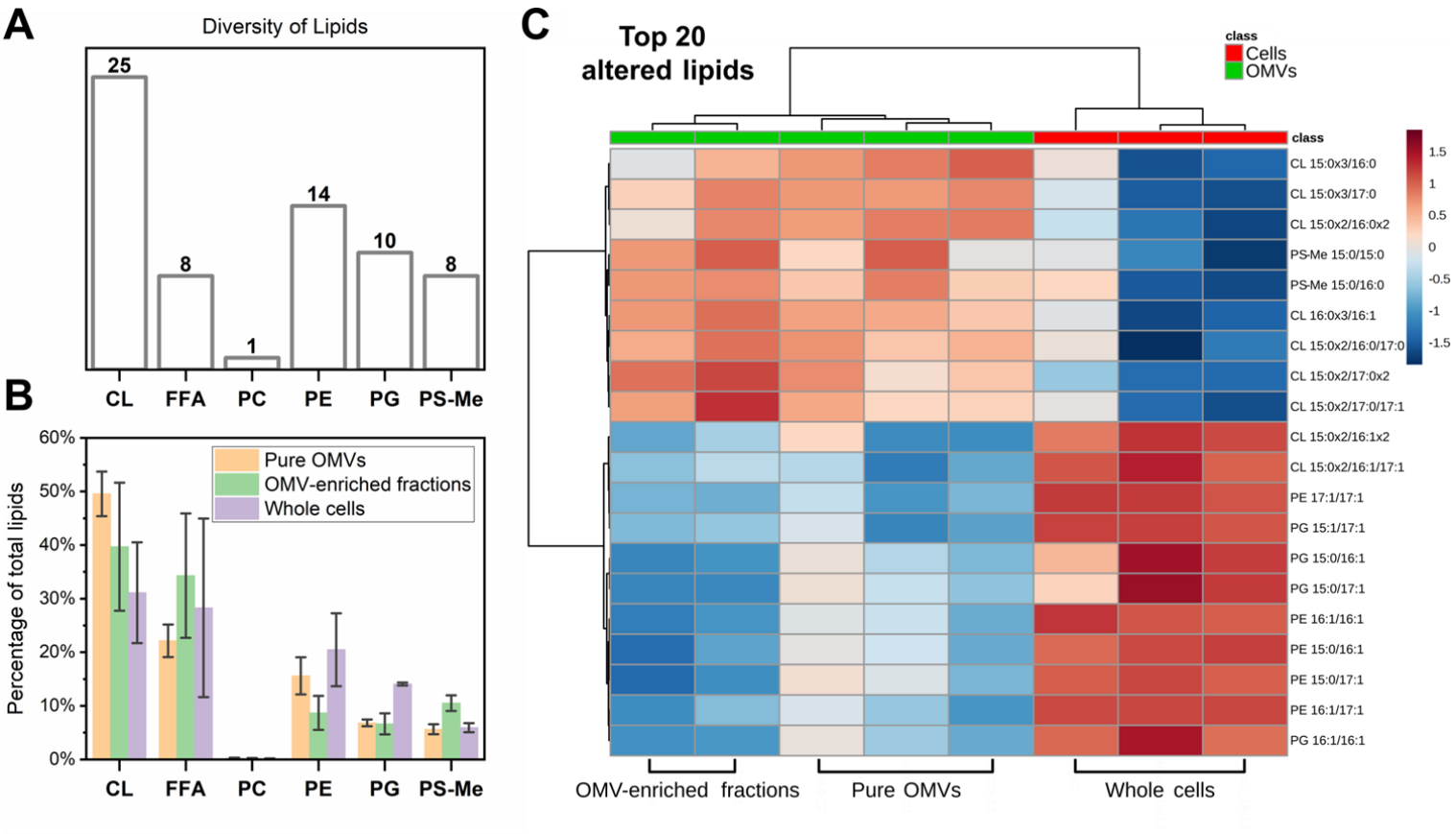

772 **Fig. 3.** Lipidomic analysis of *X. citri* whole cells and OMVs. A total of 66 different lipids
773 were identified in the samples, divided into 6 subclasses: cardiolipin (CL), free fatty acids (FFA),
774 phosphatidylcholine (PC), phosphatidylethanolamine (PE), phosphatidylglycerol (PG),
775 methylated-phosphatidylserine (PS-Me), shown in panel A. The proportion of each lipid subclass
776 varied between the different samples: Pure OMVs, OMV-enriched fractions (partially purified),
777 and whole cells (B). The 20 most altered lipids between the different samples (identified from a
778 volcano plot analysis, fold-change > 1.5, $p < 0.05$ evaluated by FDR-adjusted t-test, **Fig. S2**)
779 were clustered in a heatmap (according to one-way ANOVA), revealing the vesicles are enriched
780 in saturated cardiolipins in comparison to the cells, while being relatively impoverished in a
781 number of different unsaturated lipid species (C). The notation used to represent the lipids from
782 the different subclasses gives the number of carbon atoms and of double bonds separated by a
783 colon for each acyl chain, which in turn are separated by a slash.

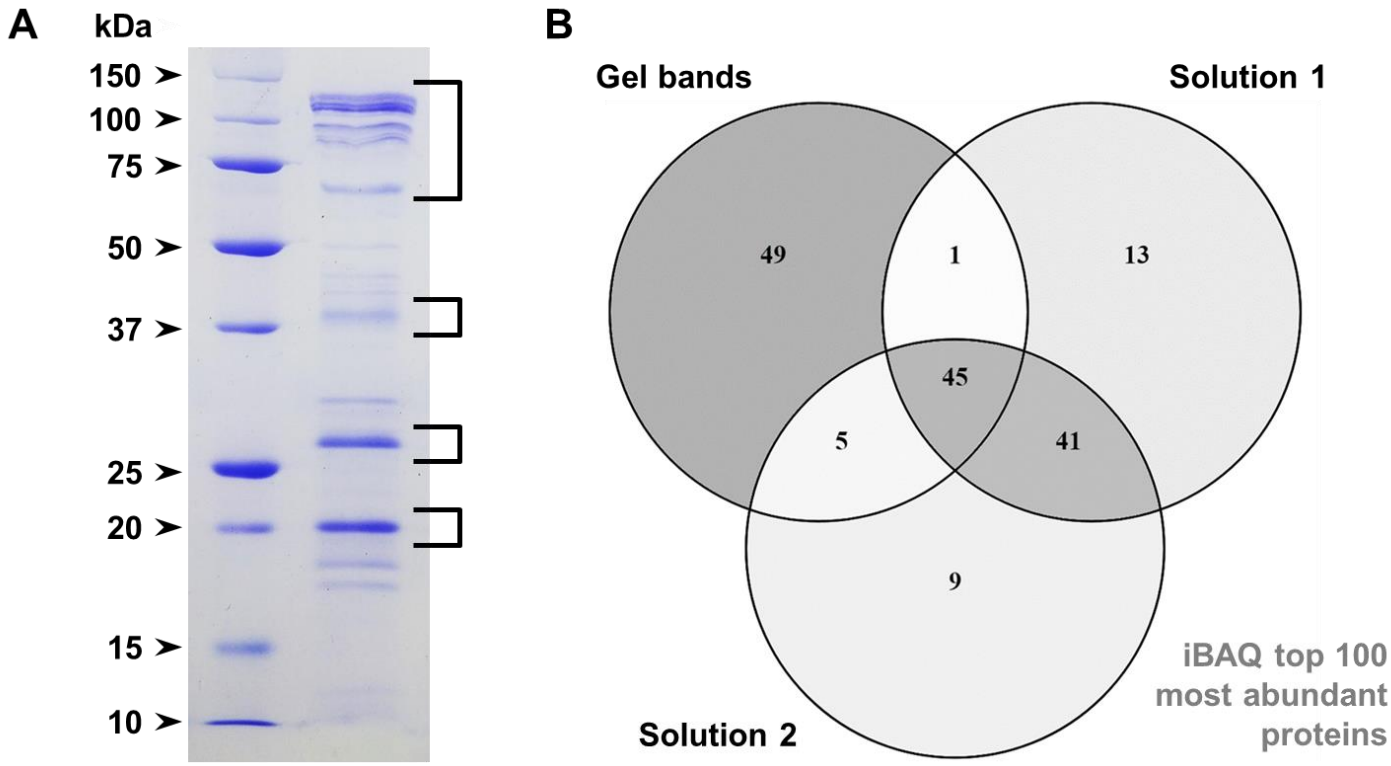

Fig. 4. Proteomic analysis of *X. citri* OMV samples. Panel A shows characteristic protein bands associated with the purified OMVs that could be observed in 15% Tris-Glycine SDS-PAGE gels. Four regions containing the main bands (square brackets) were processed by in-gel digestion for proteomic analyses; their data were combined ("gel bands") and compared to two samples of pure OMV suspensions processed by in-solution digestion ("solution 1" and "solution 2"). Panel B presents a Venn diagram displaying the intersection of the top 100 most abundant proteins for each sample determined by their iBAQ values.

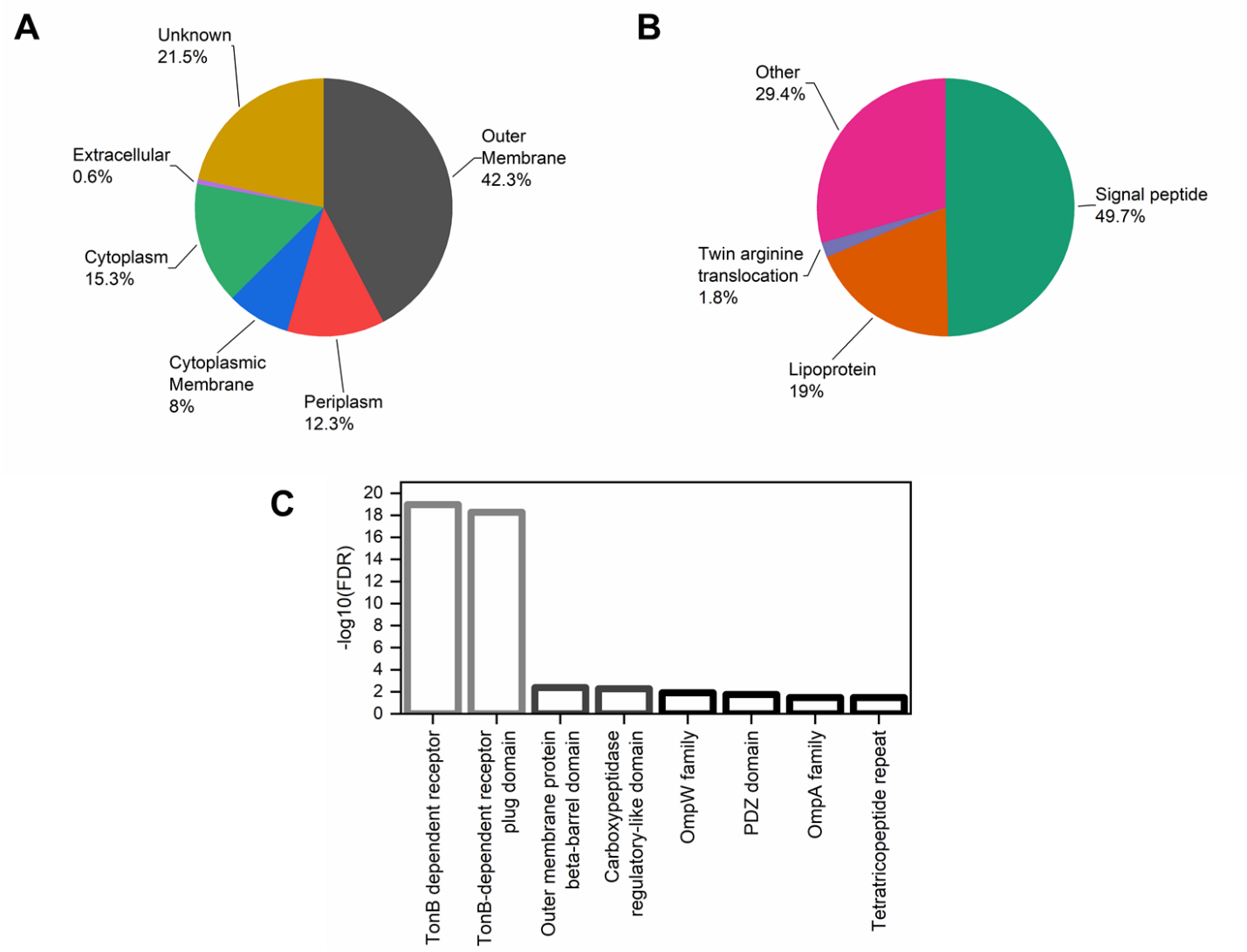

Fig. 5. Subcellular localization and domain enrichment of the most abundant proteins identified in the purified *X. citri* OMV samples. Panel A presents the subcellular protein localization predicted by PSORTb, manually curated based on sequence annotations, while panel B shows their secretion mechanisms predicted by SignalP. Panel C displays the most significantly enriched Pfam domains found in the OMVs compared to the *X. citri* pv. *citri* 306 genome. The lowest false discovery rate (FDR), thus the highest -log10(FDR), was observed for TonB-dependent receptor domains (Pfam family PF00593). These analyses were performed with

801 the combination of the top 100 proteins with the highest iBAQ values from the different samples
802 analyzed by proteomics (gel bands, solution 1, solution 2), resulting in a list of 163 non-
803 redundant proteins (**Table S1**).

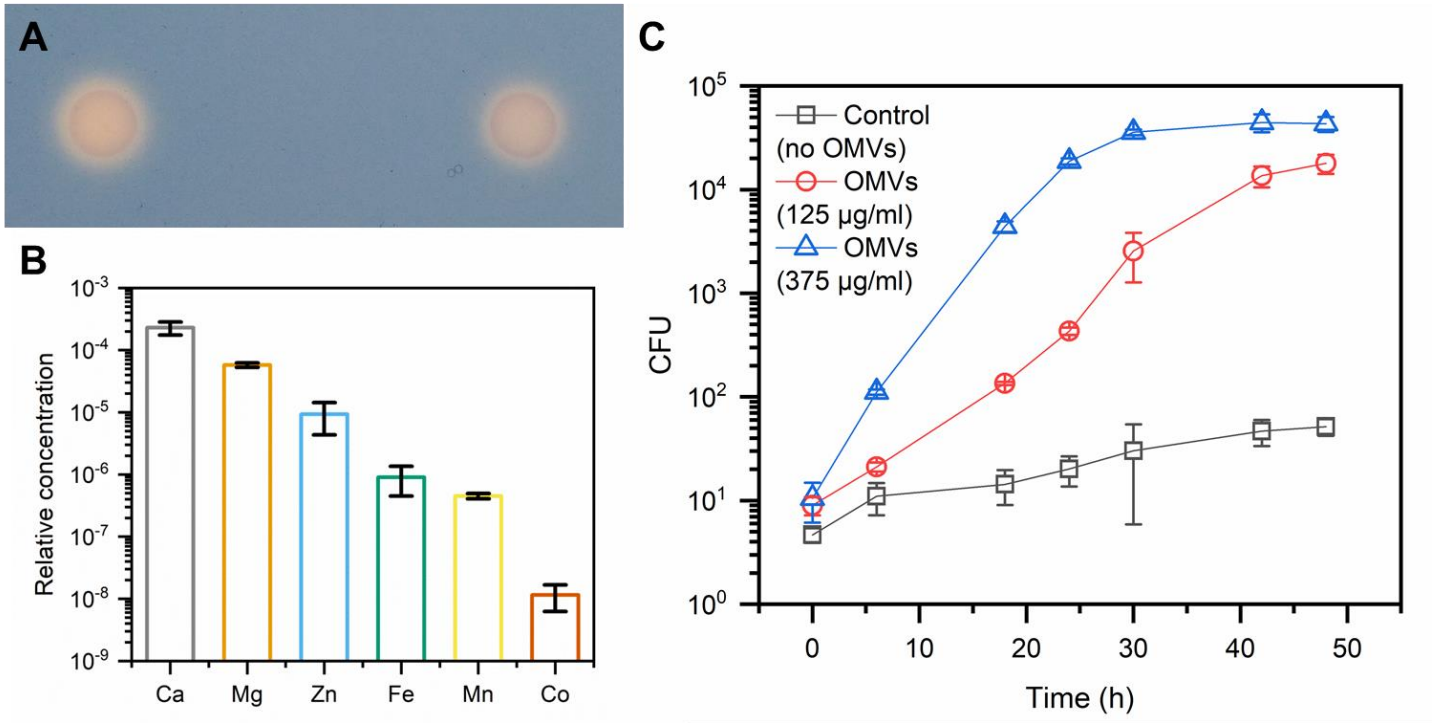

804

805 **Fig. 6.** *X. citri* OMVs carry essential metals and can be incorporated by cells.
806 Siderophores were potentially detected in the OMVs by discoloration of the medium in CAS
807 plates where vesicles were applied (A). Elemental analysis of the OMVs revealed the presence of
808 biologically important metals in the samples, including iron and zinc. The relative concentration
809 (y-axis) was calculated by the ratio between the mass fraction values for each element and the
810 carbon content. The oxidation state of each element was not determined. (B). *X. citri* can use
811 OMVs as the sole carbon source for growth, indicating that the content of the vesicles is
812 available for incorporation by cells (C). Different OMV concentrations, measured by their
813 protein content, were added to tubes with M9 medium without other carbon source and a
814 substantial increase in CFU was observed after incubation.

815

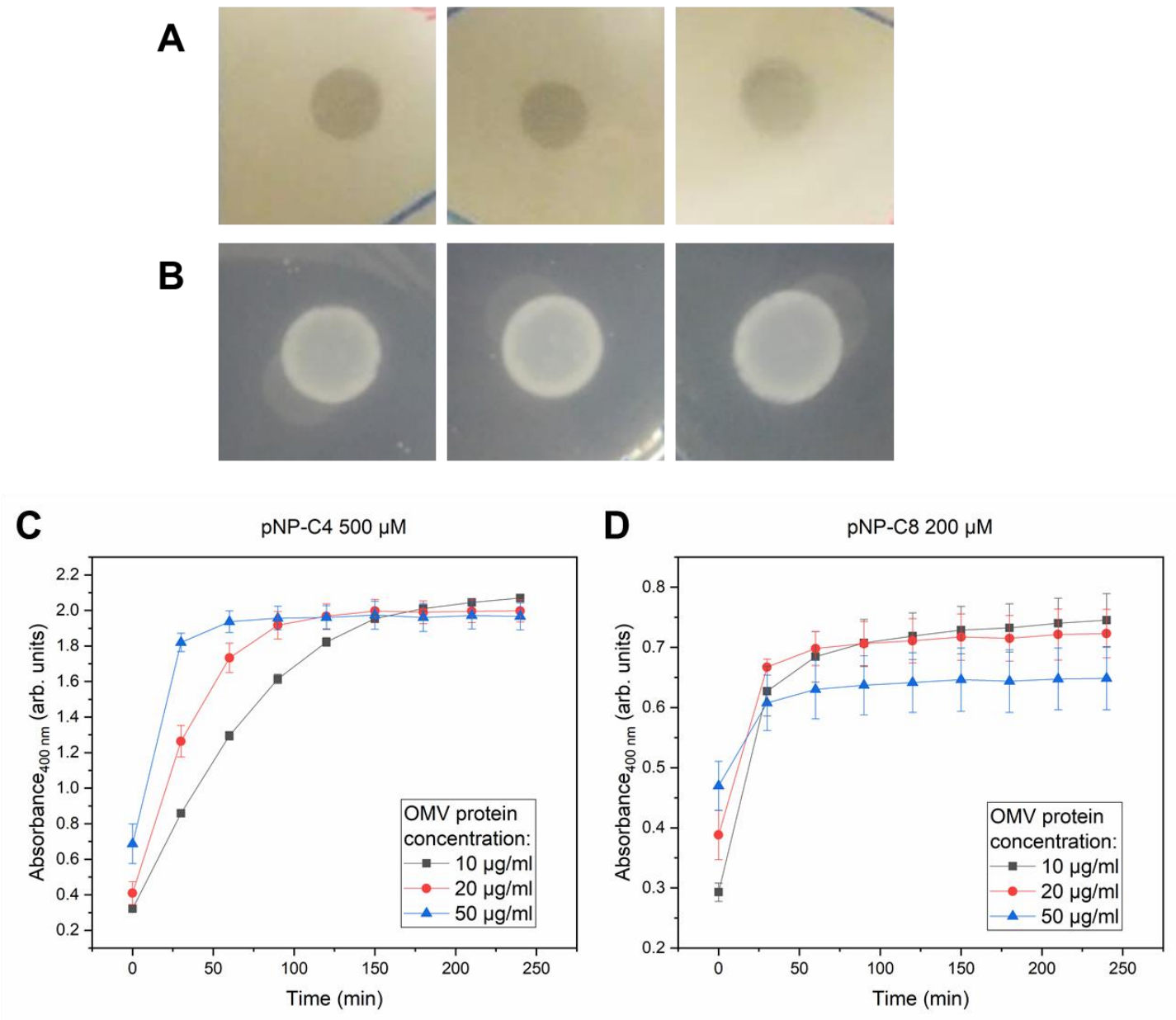

816

817 **Fig. 7.** *X. citri* OMVs present esterase activity against a broad range of substrates. In
818 qualitative esterase activity assays on agar plates, different purified OMV samples were able to
819 create a clear halo in plates emulsified with the triglyceride tributirin (A) and to generate opaque
820 white precipitates in plates containing Tween 20 and $CaCl_2$ (B). These results indicate the
821 hydrolysis of the respective substrates in the plates. Different OMV concentrations, measured by

822 their total protein content, were able to hydrolyze *p*NP-C4 (panel C) and *p*NP-C8 (panel D) in
823 colorimetric assays, indicated by the increase in absorbance at 400 nm during incubation.
824

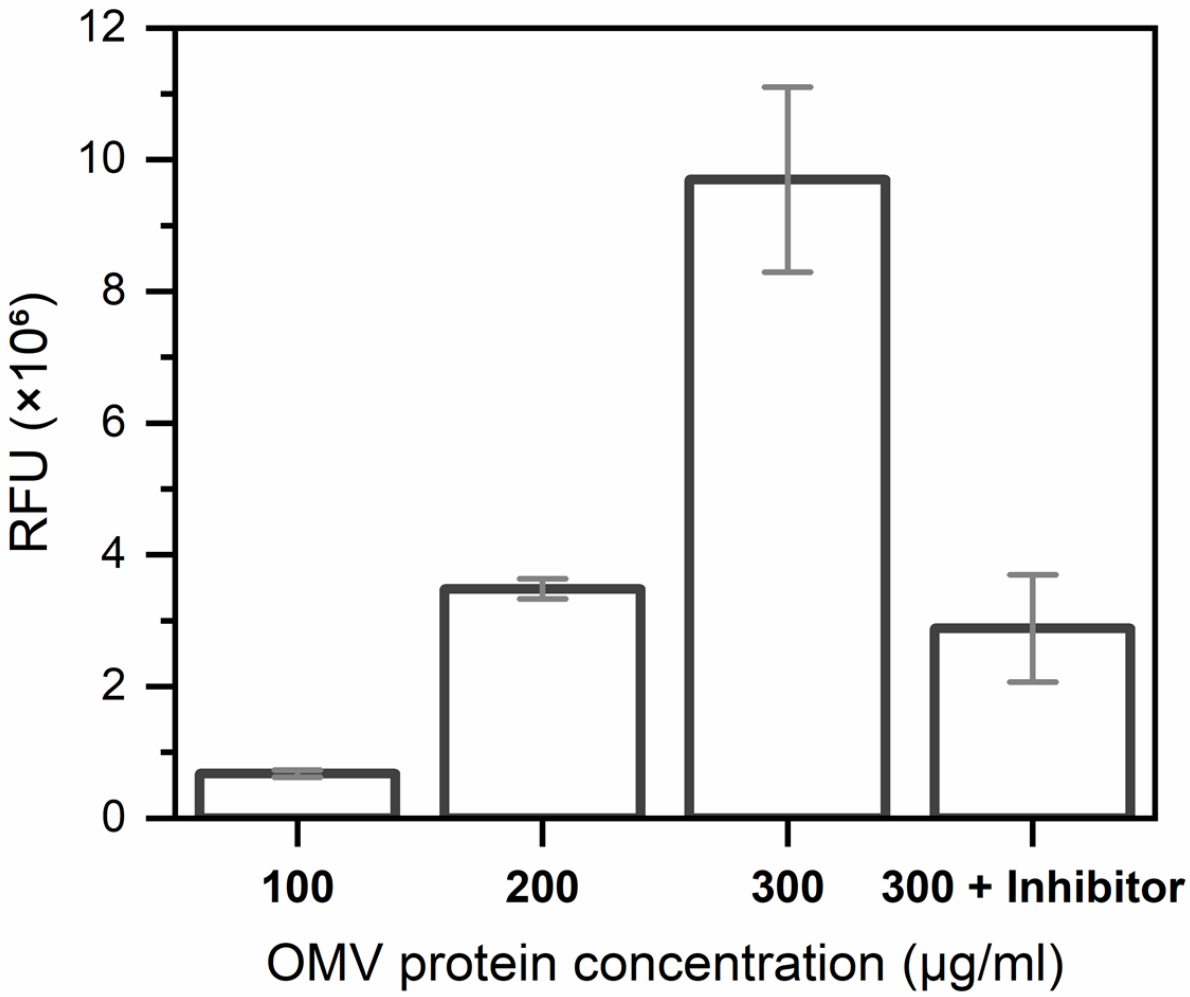

825

826 **Fig. 8.** *X. citri* OMVs present protease activity. A protease fluorescent detection kit was
827 used to detect the activity of purified OMVs at different concentrations, measured as relative
828 fluorescence units (RFU). Addition of an EDTA-free protease inhibitor to samples with the
829 highest OMV concentration tested lead to substantial decrease in the observed enzymatic
830 activity. The fluorescence from blank (phosphate buffered saline) was subtracted from all
831 samples.

832

833 **Data Set S1.** Proteomic data for purified *X. citri* OMVs, containing details of the filtered
834 proteins identified for the duplicate of in-solution digestions, including their iBAQ values
835 (XLSX file).
836
837 **Data Set S2.** Proteomic data for purified *X. citri* OMVs, containing details of the filtered
838 proteins identified for the in-gel digestion, including their iBAQ values (XLSX file).
839
840

841 **Table S1.** Combination of the top 100 most abundant proteins determined by their iBAQ
842 values from the different purified *X. citri* OMV samples (gel bands and a replicate of samples in
843 solution, **Fig. 4**), resulting in a list of 163 non-redundant proteins. UniProt annotations are
844 presented for each sequence.

UniProt ID	Gene names	Locus tags	Protein names (UniProt)	Pfam domains	InterPro domains
Q8PRF7		XAC0006	Peptidase_M48 domain-containing protein	PF01435	IPR001915
Q8PRF6		XAC0007	TPR_REGION domain-containing protein	PF13181	IPR013026; IPR011990; IPR019734
Q8PRF4	exbB	XAC0009	Biopolymer transport ExbB protein	PF01618	IPR002898
Q8PRE0	ctp	XAC0023	Carboxyl-terminal protease	PF13180; PF03572	IPR029045; IPR001478; IPR036034; IPR004447; IPR005151
Q8PRD3	egl	XAC0030	Cellulase	PF00150	IPR001547; IPR018087; IPR017853
Q8PRC7		XAC0036	Uncharacterized protein		
Q8PR40	yncD	XAC0126	Iron transporter	PF07715; PF00593	IPR039426; IPR012910; IPR037066; IPR000531; IPR036942
Q8PQZ3	fpvA	XAC0176	Ferripyoverdine receptor	PF07715; PF00593	IPR012910; IPR037066; IPR039423; IPR000531; IPR036942; IPR010105
Q8PQZ2		XAC0177	PNPLA domain-containing protein	PF01734	IPR016035; IPR002641
Q8PQX9		XAC0190	Uncharacterized protein		IPR011990
Q8PQW2	yojM	XAC0209	Superoxide dismutase [Cu-Zn] (EC 1.15.1.1)	PF00080	IPR036423; IPR024134; IPR018152; IPR001424
Q8PQU8		XAC0223	Uncharacterized protein		IPR026364; IPR023614
Q8PQT9		XAC0232	Uncharacterized protein	PF13698	IPR025294
Q8PQQ0		XAC0272	Uncharacterized protein		
Q8PQN4		XAC0289	Uncharacterized protein		IPR016980; IPR029063
Q8NL21	rplM	XAC0487	50S ribosomal protein L13	PF00572	IPR005822; IPR005823; IPR023563; IPR036899
Q8PPZ1	groL	XAC0542	60 kDa chaperonin (GroEL protein) (Protein Cpn60)	PF00118	IPR018370; IPR001844; IPR002423; IPR027409; IPR027413; IPR027410
Q8PPR2		XAC0623	Uncharacterized protein	PF04338	IPR007433
Q8PPM3	rlpA	XAC0663	Endolytic peptidoglycan transglycosylase RlpA (EC 4.2.2.-)	PF03330; PF05036	IPR034718; IPR009009; IPR036908; IPR012997; IPR007730; IPR036680
Q8PPM2	dacC	XAC0664	Serine-type D-Ala-D-Ala carboxypeptidase (EC 3.4.16.4)	PF07943; PF00768	IPR012338; IPR015956; IPR018044; IPR012907;

					IPR037167; IPR001967
Q8PPK9		XAC0677	Uncharacterized protein	PF10001	IPR018718
Q8PPK4		XAC0682	BON domain-containing protein	PF04972	IPR007055; IPR014004
Q8PPJ6	fecA	XAC0690	TonB-dependent receptor	PF07715; PF00593	IPR012910; IPR037066; IPR039423; IPR000531; IPR036942
Q8PPH0	fyuA	XAC0716	TonB-dependent receptor	PF07715; PF00593	IPR012910; IPR037066; IPR000531; IPR036942; IPR010104
Q8PPD9		XAC0747	Uncharacterized protein		IPR023614
Q8PPC1		XAC0765	Uncharacterized protein	PF04348	IPR007443; IPR028082
Q8PP23	surA	XAC0865	Chaperone SurA (Peptidyl-prolyl cis-trans isomerase SurA) (PPIase SurA) (EC 5.2.1.8) (Rotamase SurA)	PF00639; PF09312	IPR000297; IPR023034; IPR015391; IPR027304
Q8PP00	gfo	XAC0888	Glucose-fructose oxidoreductase	PF01408; PF02894	IPR004104; IPR008354; IPR036291; IPR000683
Q8PNT4	rplK	XAC0961	50S ribosomal protein L11	PF00298; PF03946	IPR000911; IPR036796; IPR006519; IPR020783; IPR036769; IPR020785; IPR020784
Q8PNS2	rplW	XAC0974	50S ribosomal protein L23	PF00276	IPR012677; IPR012678; IPR013025
Q8PNS1	rplB	XAC0975	50S ribosomal protein L2	PF00181; PF03947	IPR012340; IPR022666; IPR014722; IPR002171; IPR005880; IPR022669; IPR022671; IPR014726; IPR008991
Q8NKY0	rplV	XAC0977	50S ribosomal protein L22	PF00237	IPR001063; IPR018260; IPR036394; IPR005727
Q8PNR8	rplP	XAC0979	50S ribosomal protein L16	PF00252	IPR016180; IPR036920; IPR000114; IPR020798
Q8NL02	rplN	XAC0982	50S ribosomal protein L14	PF00238	IPR036853; IPR000218; IPR005745; IPR019972
Q8PNR4	rplE	XAC0984	50S ribosomal protein L5	PF00281; PF00673	IPR002132; IPR020930; IPR031309; IPR020929; IPR022803; IPR031310
Q8PNR3	rpsH	XAC0986	30S ribosomal protein S8	PF00410	IPR000630; IPR035987
Q8PNR1	rplR	XAC0988	50S ribosomal protein L18	PF00861	IPR005484; IPR004389
Q8PNR0	rpmD	XAC0990	50S ribosomal protein L30	PF00327	IPR036919; IPR005996; IPR016082
Q8PNQ9	rplO	XAC0991	50S ribosomal protein L15	PF00828	IPR036227; IPR030878; IPR005749; IPR001196; IPR021131
Q8NKX3	rpsM	XAC0993	30S ribosomal protein S13	PF00416	IPR027437; IPR001892; IPR010979; IPR019980; IPR018269

P0A0Y0	rpsD	XAC0995	30S ribosomal protein S4	PF00163; PF01479	IPR022801; IPR001912; IPR005709; IPR018079; IPR002942; IPR036986
Q8PNQ7	rplQ	XAC0997	50S ribosomal protein L17	PF01196	IPR000456; IPR036373
Q8PNP2	mopB	XAC1012	Outer membrane protein	PF13505; PF00691	IPR011250; IPR027385; IPR006664; IPR006665; IPR036737; IPR028974
Q8PNJ7		XAC1062	Uncharacterized protein		
Q8PNF8	slp	XAC1113	Outer membrane protein Slp	PF03843	IPR004658
Q8PND0	fyuA	XAC1143	TonB-dependent receptor	PF07715; PF00593	IPR012910; IPR039423; IPR000531; IPR036942
Q8PNB0		XAC1163	Uncharacterized protein		
Q8PN49	minE	XAC1224	Cell division topological specificity factor	PF03776	IPR005527; IPR036707
Q8PN43		XAC1230	Uncharacterized protein		IPR011256
Q8PN35		XAC1238	Endo/exonuclease/phosphatase domain-containing protein	PF03372	IPR036691; IPR005135
Q8PN33		XAC1240	Uncharacterized protein	PF13202; PF13499	IPR011992; IPR018247; IPR002048
Q8PN25	rplU	XAC1248	50S ribosomal protein L21	PF00829	IPR036164; IPR028909; IPR001787; IPR018258
Q8PMV4	mucD	XAC1321	Periplasmic serine endoprotease DegP-like (EC 3.4.21.107)	PF13180	IPR001478; IPR036034; IPR011782; IPR009003; IPR001940
Q8PMV1		XAC1324	Uncharacterized protein	PF16137	IPR032314
Q8PMS7		XAC1349	Serine protease	PF03797; PF12951; PF00082	IPR005546; IPR036709; IPR013425; IPR000209; IPR036852; IPR023827; IPR023828; IPR015500; IPR034061
Q8PMP7		XAC1379	Uncharacterized protein	PF10099	IPR018764
Q8PMM9		XAC1397	Alginate_exp domain-containing protein	PF13372	IPR025388
Q8PML3	oma	XAC1413	Outer membrane protein assembly factor BamA	PF01103; PF07244	IPR000184; IPR010827; IPR039910; IPR023707; IPR034746
Q8PMJ3		XAC1434	CASH domain-containing protein	PF13229	IPR039448; IPR006633; IPR022441; IPR006626; IPR012334; IPR011050
Q8PMJ2	fhuA	XAC1435	Iron receptor	PF07715; PF00593	IPR012910; IPR037066; IPR039423; IPR000531; IPR036942; IPR010917; IPR010105
Q8PMH2	dcp	XAC1456	Peptidyl-dipeptidase	PF01432	IPR034005; IPR024077; IPR001567
Q8PMG5		XAC1463	Phospholipase A1 (EC 3.1.1.32) (EC	PF02253	IPR003187; IPR036541

			3.1.1.4) (Phosphatidylcholine 1-acylhydrolase)		
Q8PMG3	pcp	XAC1466	Peptidoglycan-associated outer membrane lipoprotein	PF05433	IPR008816
Q8PMF0		XAC1479	OmpA family protein	PF13488; PF00691	IPR039567; IPR006664; IPR006665; IPR006690; IPR036737
Q8PMD2		XAC1497	Uncharacterized protein		
Q8PMB6	smpA	XAC1516	Outer membrane protein assembly factor BamE	PF04355	IPR026592; IPR037873; IPR007450
Q8PM83	btuE	XAC1549	Glutathione peroxidase	PF00255	IPR000889; IPR029759; IPR036249
Q8PM82	fkpA	XAC1550	Peptidyl-prolyl cis-trans isomerase (EC 5.2.1.8)	PF00254; PF01346	IPR001179; IPR000774; IPR036944
Q8PM54	oprO	XAC1579	Polyphosphate-selective porin O	PF07396	IPR023614; IPR010870
Q8NL26		XAC1585	Peptidyl-prolyl cis-trans isomerase (EC 5.2.1.8)	PF00254; PF01346	IPR001179; IPR000774; IPR036944
Q8PM13	rpsR	XAC1621	30S ribosomal protein S18	PF01084	IPR001648; IPR018275; IPR036870
Q8PLS7		XAC1712	DUF218 domain-containing protein	PF02698	IPR003848; IPR014729
Q8PLR1	nlpD	XAC1728	Lipoprotein	PF01476; PF01551	IPR011055; IPR018392; IPR036779; IPR016047
Q8PLN4		XAC1761	Uncharacterized protein		
Q8PL93	cirA	XAC1910	TonB-dependent receptor	PF07715; PF00593	IPR012910; IPR037066; IPR000531; IPR010104
Q8PKZ8	lolA	XAC2008	Outer-membrane lipoprotein carrier protein	PF03548	IPR029046; IPR004564; IPR018323
Q8PKZ0	pilF	XAC2017	Fimbrial biogenesis protein		IPR013360; IPR013026; IPR011990; IPR019734
Q8PKY7	bamB	XAC2020	Outer membrane protein assembly factor BamB	PF13360	IPR017687; IPR018391; IPR002372; IPR011047; IPR015943
Q8PK64		XAC2312	TonB_dep_Rec domain-containing protein	PF00593	IPR039426; IPR013784; IPR000531
Q8PK57		XAC2319	Uncharacterized protein		
Q8PK24		XAC2353	Uncharacterized protein		
Q8PJM6	rpfN	XAC2504	Porin	PF04966	IPR007049; IPR038673
Q8PJK8	ggt	XAC2523	Gamma-glutamyltranspeptidase		IPR043138; IPR000101; IPR043137; IPR029055
Q8PJK6		XAC2525	Uncharacterized protein		
Q8PJK0	btuB	XAC2531	TonB-dependent receptor	PF07715; PF00593	IPR012910; IPR037066; IPR000531; IPR010916
Q8PJH0		XAC2562	Uncharacterized protein		
Q8PJE3	rplT	XAC2591	50S ribosomal protein L20	PF00453	IPR005813; IPR035566
Q8PJD5	btuB	XAC2600	TonB-dependent receptor	PF07715	IPR012910; IPR037066; IPR010104; IPR010917

Q8PJC4		XAC2611	DUF4189 domain-containing protein	PF13827	IPR025240
Q8PJB5	virB9	XAC2620	VirB9 protein	PF03524	IPR010258; IPR033645; IPR038161
Q8PJ70	oar	XAC2672	Oar protein		IPR039426; IPR008969; IPR036942
Q8PJ58	rpsO	XAC2684	30S ribosomal protein S15	PF00312	IPR000589; IPR005290; IPR009068
Q8PJ03	btuB	XAC2742	TonB-dependent receptor	PF07715; PF00593	IPR012910; IPR037066; IPR000531; IPR010917
Q8PJ02	oar	XAC2743	Oar protein	PF07715; PF00593	IPR039426; IPR013784; IPR012910; IPR037066; IPR000531
Q8PIY6	phoA	XAC2759	Alkaline phosphatase	PF00245	IPR001952; IPR017850
Q8PIX3	bp26	XAC2772	Outer membrane protein	PF04402	IPR007497
Q8PIX2	oar	XAC2773	Oar protein	PF07715; PF00593	IPR039426; IPR013784; IPR012910; IPR037066; IPR000531
Q8PIW5	rlpB	XAC2780	LPS-assembly lipoprotein LptE	PF04390	IPR007485
Q8PIU4		XAC2801	Uncharacterized protein	PF06629	IPR010583
Q8PIR6	phuR	XAC2829	Outer membrane hemin receptor	PF07715; PF00593	IPR039426; IPR012910; IPR037066; IPR000531; IPR036942
Q8PIF7	fhuA	XAC2941	TonB-dependent receptor	PF07715; PF00593	IPR012910; IPR037066; IPR039423; IPR000531; IPR036942; IPR010105
Q8PIF2		XAC2946	Uncharacterized protein	PF10670	IPR019613
Q8PIE7	comEA	XAC2951	DNA transport competence protein		IPR004509; IPR010994
Q8PIE0		XAC2958	Uncharacterized protein	PF09839	IPR018642
Q8PID5		XAC2963	Uncharacterized protein	PF11306	IPR021457
Q8PI48	btuB	XAC3050	TonB-dependent receptor	PF07715; PF00593	IPR012910; IPR037066; IPR000531; IPR036942
Q8PI41	bla	XAC3057	Beta-lactamase	PF00144	IPR001466; IPR012338
Q8PI27	iroN	XAC3071	TonB-dependent receptor	PF07715; PF00593	IPR012910; IPR037066; IPR000531; IPR010104
Q8PHZ0		XAC3108	Uncharacterized protein		IPR011990
Q8PHV9	cpoB	XAC3140	Cell division coordinator CpoB	PF16331; PF13525	IPR039565; IPR034706; IPR014162; IPR013026; IPR011990; IPR019734; IPR032519
Q8PHV8	ompP6	XAC3141	Peptidoglycan-associated protein	PF00691	IPR006664; IPR006665; IPR036737; IPR039001; IPR014169
Q8PHV7	tolB	XAC3142	Tol-Pal system protein TolB	PF07676; PF04052	IPR011042; IPR011659; IPR014167; IPR007195; IPR036752
Q8PHV5	tolR	XAC3144	Tol-Pal system protein TolR	PF02472	IPR003400; IPR014168

Q8PHV4	tolQ	XAC3145	Tol-Pal system protein TolQ	PF01618	IPR002898; IPR014163
Q8PHU4		XAC3155	Uncharacterized protein	PF11218	IPR021381
Q8PHT7	bla	XAC3162	Beta-lactamase (EC 3.5.2.6)		IPR012338; IPR000871; IPR023650; IPR006311
Q8PHT1	bfeA	XAC3168	Ferric enterobactin receptor	PF07715; PF00593	IPR012910; IPR037066; IPR000531; IPR010916; IPR036942
Q8PHT0	bfeA	XAC3169	Ferric enterobactin receptor	PF07715; PF00593	IPR012910; IPR037066; IPR000531; IPR036942
Q8PHS3	fecA	XAC3176	Citrate-dependent iron transporter	PF07715; PF00593	IPR012910; IPR037066; IPR000531; IPR036942; IPR010105
Q8PHQ5	btuB	XAC3194	Outer membrane receptor for transport of vitamin B	PF07715; PF00593	IPR010101; IPR039426; IPR012910; IPR037066; IPR000531; IPR036942
Q8PHP1	bfeA	XAC3207	Ferric enterobactin receptor	PF07715; PF00593	IPR012910; IPR037066; IPR000531; IPR010916; IPR036942
Q8PHN1	comL	XAC3218	Outer membrane protein assembly factor BamD	PF13525	IPR017689; IPR039565; IPR013026; IPR011990
Q8PHL0	fimA	XAC3241	Fimbrillin	PF07963; PF00114	IPR012902; IPR001082
Q8PHF7	estA	XAC3300	Lipase	PF03797; PF00657	IPR005546; IPR036709; IPR001087; IPR017186; IPR036514
Q8PHE6	iroN	XAC3311	TonB-dependent receptor	PF07715; PF00593	IPR012910; IPR037066; IPR006311; IPR000531; IPR036942; IPR010104
Q8PHC5	fecA	XAC3334	TonB-dependent receptor	PF07715; PF00593	IPR039426; IPR012910; IPR037066; IPR000531; IPR036942
Q8PHA8		XAC3351	Uncharacterized protein		
Q8PHA5	ompW	XAC3354	Outer membrane protein W	PF03922	IPR011250; IPR005618
Q8PHA4	omp21	XAC3355	Outer membrane protein	PF03922	IPR011250; IPR005618
Q8PH89	fhuE	XAC3370	Outer membrane receptor for ferric iron uptake	PF07715; PF00593	IPR012910; IPR037066; IPR039423; IPR000531; IPR036942; IPR010105
Q8PH16	btuB	XAC3444	TonB-dependent receptor	PF07715; PF00593	IPR012910; IPR037066; IPR000531; IPR036942
Q8PGZ9	tolC	XAC3463	TolC protein	PF02321	IPR003423; IPR010130
Q8PGZ0	oprO	XAC3472	Polyphosphate-selective porin O	PF07396	IPR023614; IPR010870
Q8PGX3	fyuA	XAC3489	TonB-dependent receptor	PF07715; PF00593	IPR012910; IPR037066; IPR039423; IPR000531; IPR036942
Q8PGW4	fhuE	XAC3498	Outer membrane receptor for ferric iron uptake	PF07715; PF00593	IPR012910; IPR037066; IPR039423; IPR000531;

					IPR036942; IPR010917; IPR010105
Q8PGU1		XAC3525	Uncharacterized protein		
Q8PGL1	uptE	XAC3605	Outer membrane protein		IPR036737
Q8PGL0	uptD	XAC3606	Outer membran protein	PF14346	IPR025511
Q8PGJ6	pfeA	XAC3620	Siderophore receptor protein	PF07715; PF00593	IPR039426; IPR012910; IPR037066; IPR000531; IPR036942; IPR010917; IPR010105
Q8PGG6	atpG	XAC3650	ATP synthase gamma chain (ATP synthase F1 sector gamma subunit)	PF00231	IPR035968; IPR000131; IPR023632
Q8PGG0		XAC3657	Uncharacterized protein		IPR011250
Q8PGF7		XAC3660	Uncharacterized protein		
Q8PGF3	ompW	XAC3664	Outer membrane protein	PF03922	IPR011250; IPR005618
Q8PGF0		XAC3667	Lipoprotein	PF03180	IPR004872
Q8PGC9	dadA	XAC3688	D-amino acid dehydrogenase (EC 1.4.99.-)	PF01266	IPR023080; IPR006076; IPR036188
Q8PFX5	amaA	XAC3847	N-acyl-L-amino acid amidohydrolase	PF07687; PF01546	IPR017439; IPR036264; IPR002933; IPR011650
Q8PFW2		XAC3860	N-acetylmuramoyl-L-alanine amidase	PF01510	IPR036505; IPR002502
Q8PFV4	yliI	XAC3868	Dehydrogenase	PF07995	IPR011042; IPR012938; IPR011041
P66535	rpsU	XAC3872	30S ribosomal protein S21	PF01165	IPR001911; IPR018278; IPR038380
Q8PFR1		XAC3917	SPOR domain-containing protein	PF05036	IPR007730; IPR036680
Q8PFQ2		XAC3926	OMP_b-brl domain-containing protein	PF13505	IPR011250; IPR027385
Q8PFK1	htrA	XAC3980	Periplasmic serine endoprotease DegP-like (EC 3.4.21.107)	PF13180	IPR001478; IPR036034; IPR011782; IPR009003; IPR001940
Q8PFK0		XAC3981	Uncharacterized protein		
Q8PFH3	ecnA	XAC4008	Entericidin A	PF08085	IPR012556
Q8PFD5	iroN	XAC4048	TonB-dependent receptor	PF07715; PF00593	IPR012910; IPR037066; IPR000531; IPR010104
P66160	rpmB	XAC4159	50S ribosomal protein L28	PF00830	IPR034704; IPR026569; IPR037147; IPR001383
Q8PEX1		XAC4219	Ysc84 domain-containing protein	PF04366	IPR007461
Q8PER7		XAC4273	OmpA-related protein	PF00593	IPR039426; IPR013784; IPR000531
Q8PER6		XAC4274	OmpA-related protein	PF00593	IPR039426; IPR013784; IPR000531
Q8PEK7	yrbC	XAC4342	Toluene tolerance protein	PF05494	IPR008869; IPR042245
Q8PEK5	vacJ	XAC4344	Lipoprotein	PF04333	IPR007428
Q8PRJ3	virB9	XACb0039	VirB9 protein	PF03524	IPR010258; IPR014148; IPR033645; IPR038161
Q8NL05	rpsN		30S ribosomal protein S14	PF00253	IPR001209; IPR043140; IPR023036

845 **Table S2.** Results from the TQ ICP-MS elemental analysis of samples containing
846 purified OMV suspended in PBS. The data for **Fig. 6B** were obtained by subtracting the
847 background concentration of each element in PBS and normalizing the values for each sample
848 based on their respective carbon content. See also **Table S3** and **Table S4** for experimental
849 details. LOD: limit of detection.

Element	**Buffer PBS 1×**	**Sample 1**	**Sample 2**	**Sample 3**	**LOD**	**Unit**
C	< LOD	776 ± 13	1285 ± 3	899 ± 2	24.8	**mg L^{-1}**
Mg	< LOD	41.4 ± 0.6	80.6 ± 1.0	51.2 ± 1.0	0.295	µg L^{-1}
S	80 ± 1	112 ± 2	152 ± 3	113 ± 2	0.473	µg L^{-1}
Ca	47 ± 1	273 ± 3	292 ± 10	232 ± 6	6.782	µg L^{-1}
Mn	0.09 ± 0.01	0.43 ± 0.01	0.62 ± 0.03	0.54 ± 0.01	0.007	µg L^{-1}
Fe	1.58 ± 0.14	2.13 ± 0.03	2.32 ± 0.10	2.85 ± 0.14	0.196	µg L^{-1}
Co	0.044 ± 0.003	0.053 ± 0.005	0.052 ± 0.003	0.059 ± 0.006	0.001	µg L^{-1}
Ni	0.48 ± 0.02	3.08 ± 0.09	0.96 ± 0.06	0.97 ± 0.10	0.154	µg L^{-1}
Cu	< LOD	0.132 ± 0.002	< LOD	< LOD	0.037	µg L^{-1}
Zn	1.06 ± 0.03	6.97 ± 0.10	8.04 ± 0.15	14.57 ± 0.12	0.175	µg L^{-1}
Br	153 ± 8	136 ± 14	149 ± 11	138 ± 7	0.042	µg L^{-1}
Se	< LOD	< LOD	0.004 ± 0.001	< LOD	0.002	µg L^{-1}
Ba	1.01 ± 0.03	1.15 ± 0.01	1.49 ± 0.02	1.27 ± 0.02	0.003	µg L^{-1}

850

851 **Table S3.** Mass values defined in the quadrupoles for the TQ ICP-MS elemental analysis.

Element	Isotope	Analysis Mode	Q_1 mass	Q_2 filled with	Q_3 mass	LOD	Unit	Linear Range	Sensitivity (cps L μg^{-1})	R^2
C	12	SQ - KED	---	Helium	12	24.8	**mg L^{-1}**	50 - 1500	3.0×10^2	0.9999
Mg	24	SQ - KED	---	Helium	24	0.295	µg L^{-1}	25 - 100	6.3×10^2	0.9924
S	32	TQ - O2	32	Oxygen	48 ($^{32}S.^{16}O^+$)	0.473	µg L^{-1}	3 - 160	1.9×10^3	0.9987
Ca	44	SQ - KED	---	Helium	44	6.782	µg L^{-1}	25 - 500	4.5×10^1	0.9997
Mn	55	SQ - KED	---	Helium	55	0.007	µg L^{-1}	0.01 - 5	9.2×10^3	0.9999
Fe	57	SQ - KED	---	Helium	57	0.196	µg L^{-1}	0.25 - 5	4.1×10^2	0.9977
Co	59	SQ - KED	---	Helium	59	0.001	µg L^{-1}	0.01 - 1	3.8×10^4	0.9993
Ni	60	SQ - KED	---	Helium	60	0.154	µg L^{-1}	0.25 - 10	1.2×10^4	0.9939
Cu	63	SQ - KED	---	Helium	63	0.037	µg L^{-1}	0.05 - 10	3.1×10^4	0.9999
Zn	66	SQ - KED	---	Helium	66	0.175	µg L^{-1}	0.25 - 25	4.1×10^3	0.9997
Br	79	TQ - O2	79	Oxygen	95 ($^{79}Br.^{16}O^+$)	0.042	µg L^{-1}	50 - 500	3.6×10^2	0.9999
Se	80	TQ - O2	80	Oxygen	96 ($^{80}Se.^{16}O^+$)	0.002	µg L^{-1}	0.005 - 1	2.1×10^3	0.9993
Ba	138	TQ - O2	138	Oxygen	154 ($^{138}Ba.^{16}O^+$)	0.003	µg L^{-1}	0.05 - 5	5.2×10^4	0.9999

852

853

854 **Table S4.** TQ ICP-MS operating conditions.

RF Power (W)	**1550**
Argon coolant gas flow (L min^{-1})	14
Argon auxiliary gas flow (L min^{-1})	0.8
Argon nebulizer flow (L min^{-1})	1.04
He flow gas (mL min^{-1})	6.57
O_2 flow gas (mL min^{-1})	0.6
Nebulizer	MicroMist U-Series 0.4 mL min^{-1}
Spray Chamber	Glass Cyclonic spray chamber
Peristaltic Pump (rpm)	40
Spray chamber temperature (℃)	2.7
Dwell time (s)	0.1
Number of Sweeps	10

855

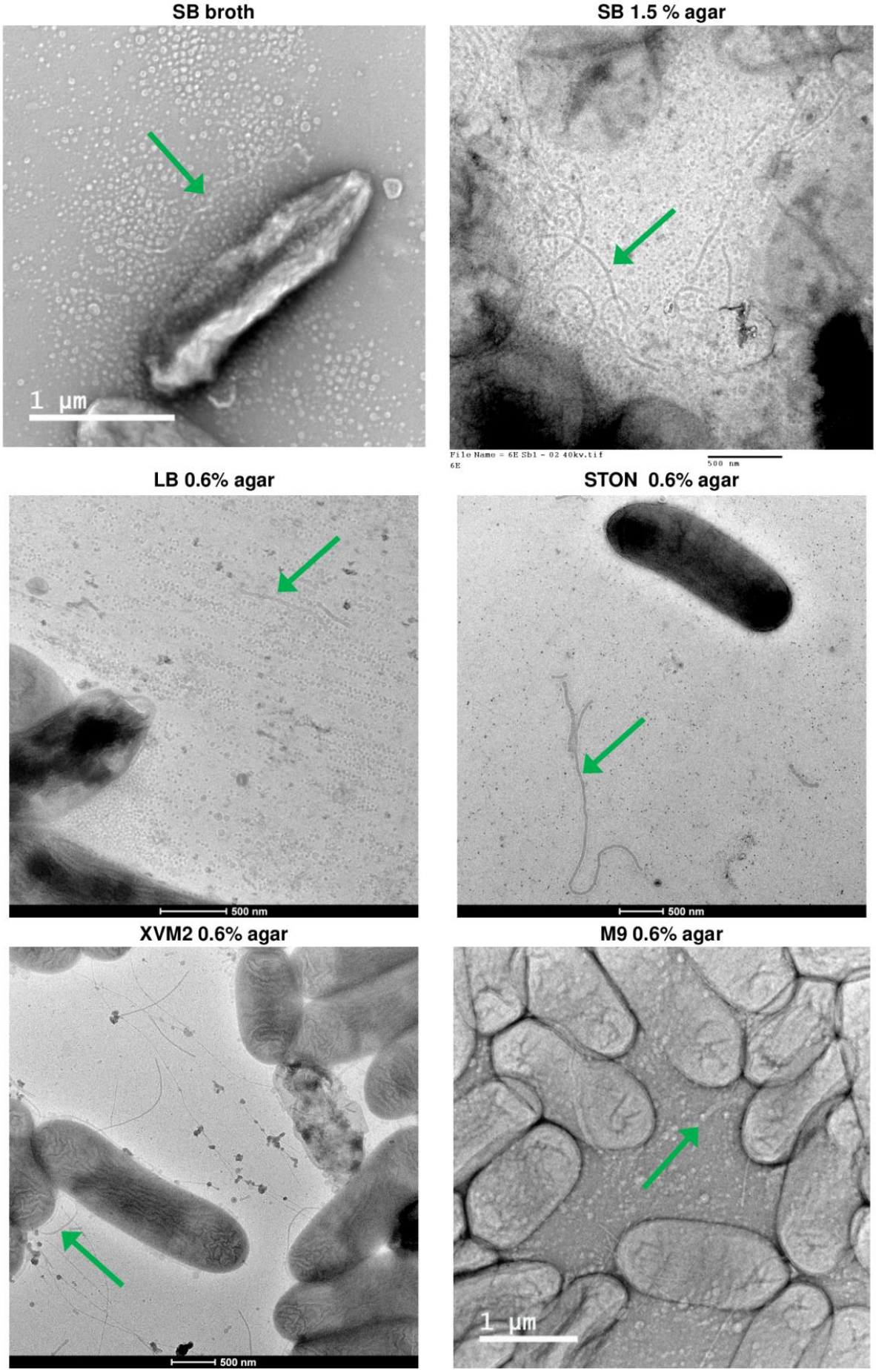

856

857 **Fig. S1.** Formation of outer membrane tubes by *X. citri* cells in different culture
858 conditions and media. The tested media include liquid SB, in which the samples were
859 concentrated by ultracentrifugation before being applied to the TEM grids, SB with 1.5% agar (a
860 higher concentration than the 0.6% used for Fig. 1), LB with 0.6% agar, STON with 0.6% agar
861 (Guzzo et al., J Mol Biol, 2009, 10.1016/j.jmb.2009.07.065), XVM2 with 0.6% agar (Wengelnik
862 et al., J Bacteriol, 1996, 10.1128/jb.178.4.1061-1069.1996), and M9 with 0.6% agar. The green
863 arrows point to examples of the outer membrane tubes that can be seen in the images.
864

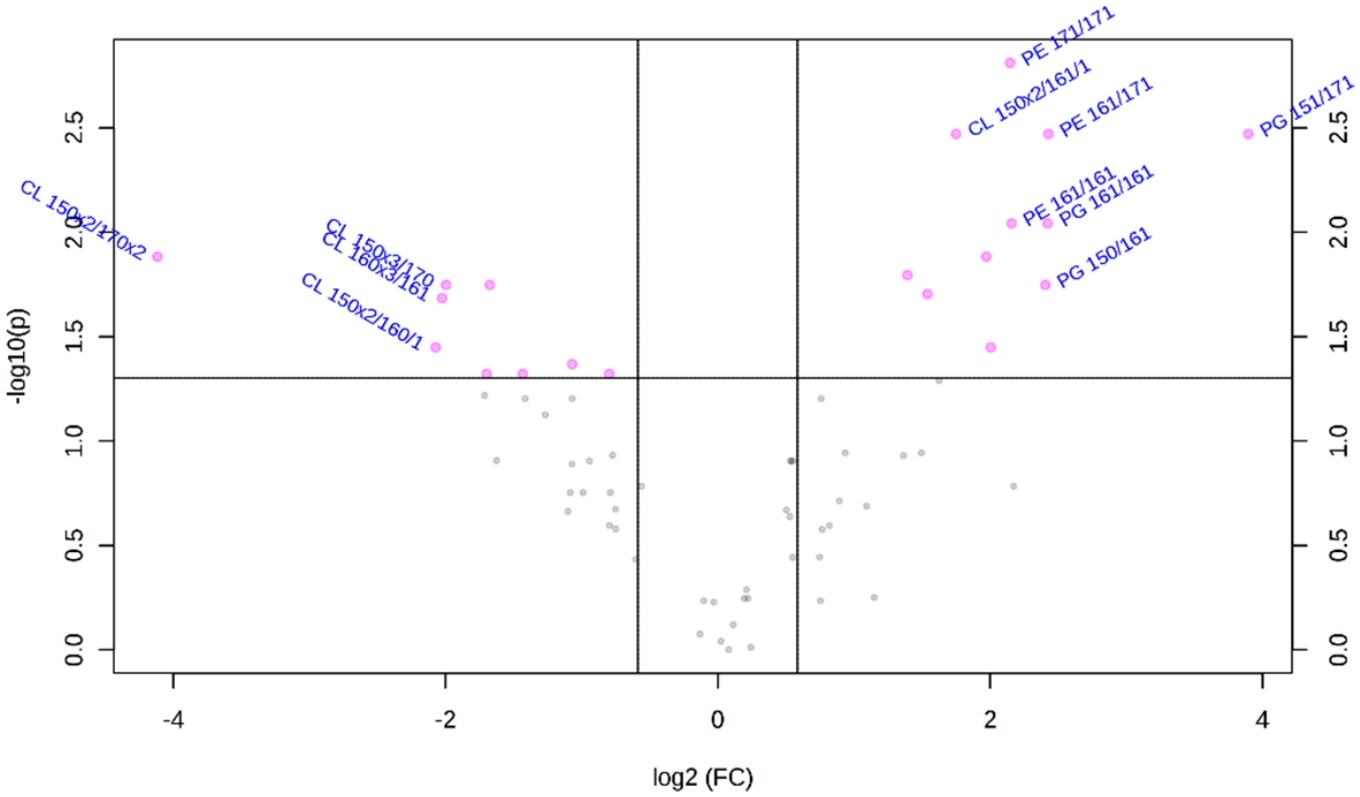

865

866 **Fig. S2.** Volcano plot analysis of the lipidomic data. The 20 most altered lipids between
867 the OMV and whole cell samples are identified in the plot as the ones presenting fold change
868 values above 1.5 and $p<0.05$. Statistical significance was evaluated by FDR-adjusted t-test.

869

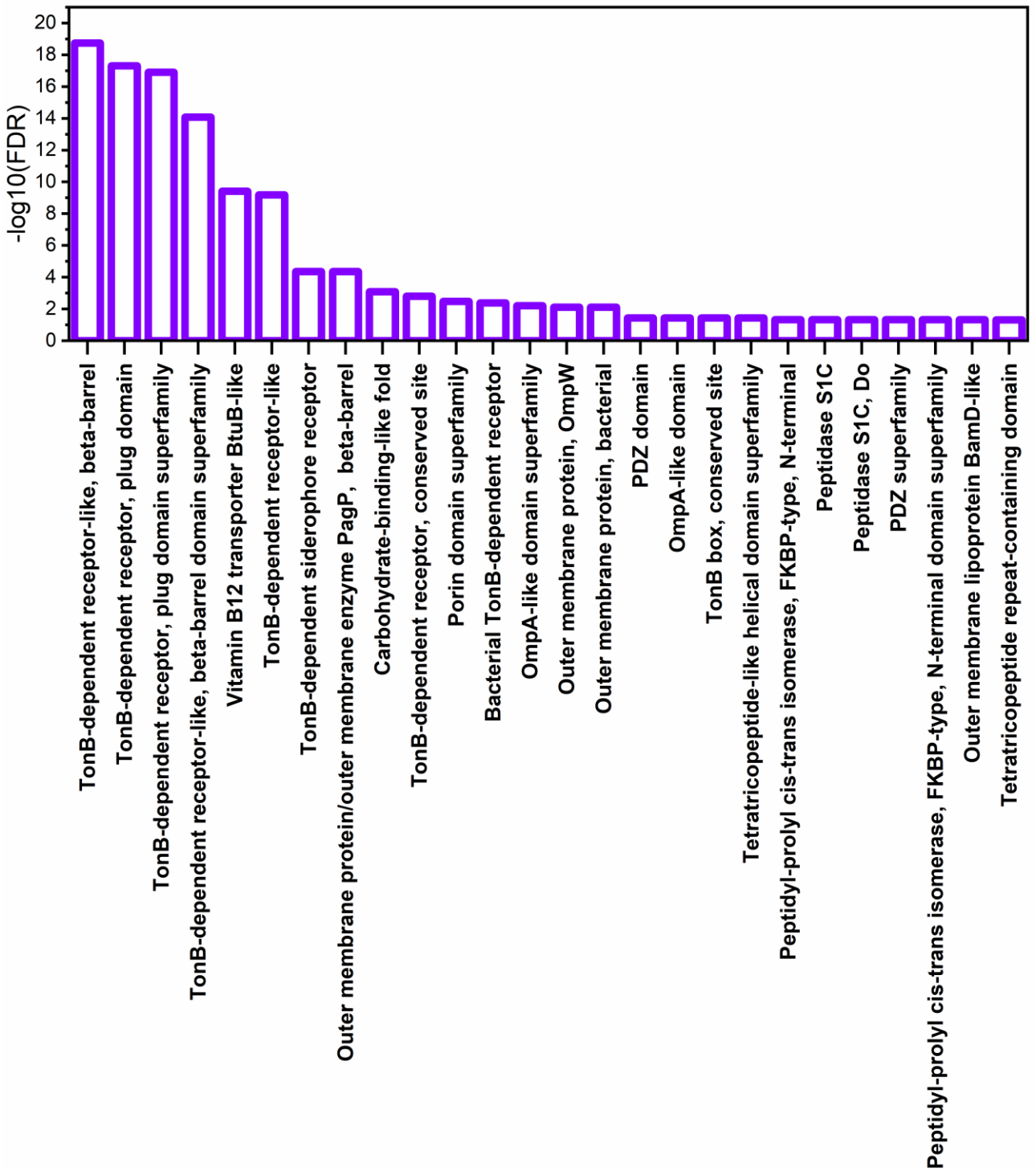

870

871 **Fig. S3.** Most significantly enriched InterPro domains found in the purified OMVs
872 compared to the *X. citri* pv. *citri* 306 genome. The lowest false discovery rates (FDR), thus the
873 highest -log10(FDR) values, were observed for domains related to TonB-dependent receptors.